6-13-2007

Description of harmonic generation in terms of the complex quasienergy. II. Application to time-dependent effective range theory

M.V. Frolov
Voronezh State University, Voronezh 394006, Russia

A.V. Flegel
Voronezh State University, Voronezh 394006, Russia

N. L. Manakov
Voronezh State University, manakov@phys.vsu.ru

Anthony F. Starace
University of Nebraska-Lincoln, astarace1@unl.edu

Description of harmonic generation in terms of the complex quasienergy. II. Application to time-dependent effective range theory

M. V. Frolov, A. V. Flegel, and N. L. Manakov
Department of Physics, Voronezh State University, Voronezh 394006, Russia

Anthony F. Starace
Department of Physics and Astronomy, University of Nebraska, Lincoln, Nebraska 68588-0111, USA
(Received 16 January 2007; published 7 June 2007; corrected 13 June 2007)

A formulation for the high-order harmonic generation (HHG) amplitude [M. V. Frolov *et al.*, Phys. Rev. A **75**, 063407 (2007), preceding paper] is employed to provide analytical results for HHG rates within our recently developed time-dependent effective range (TDER) theory (for time-dependent problems involving weakly bound electron systems). Exact and approximate (including quasiclassical) TDER HHG rates are employed to analyze the accuracy of common approximate methods for HHG calculations. For various specific negative ions with *s* and *p* outer electrons, numerical results for HHG spectra are presented over a wide interval of laser frequencies (extending from the tunneling to the multiphoton regimes). The role of initial bound state symmetry effects on the HHG spectra is also analyzed. Finally, Coulomb corrections to TDER results for HHG rates are introduced and discussed.

DOI: 10.1103/PhysRevA.75.063408 PACS number(s): 32.80.Wr, 42.50.Hz, 42.65.Ky

I. INTRODUCTION

The *ab initio* formulation of high-order harmonic generation (HHG) rates in our preceding paper [1] (hereafter referred to as paper I) in terms of the complex quasienergy is a very general one that is applicable to any atomic system. In practice, this formulation requires a manageable expression for the complex quasienergy of a system regarded as a function of two fields: a strong fundamental field of frequency ω and a weak probe field having harmonic frequency $N\omega$. As we show in the present paper, this formulation allows one to obtain essentially analytical results for HHG rates within the time-dependent effective range (TDER) theory of strong laser processes [2,3], which is appropriate for the description of an electron bound in a short-range potential.

Direct numerical solutions of the time-dependent Schrödinger equation are time consuming and do not allow one to trace in detail the features of strong laser-atom phenomena over a wide range of laser parameters. On the other hand, classical and semiclassical theories as well as exactly solvable quantum models have proved to be effective for analyzing qualitative features of laser-atom interactions in the strong-field regime (see, e.g., the review [4]). The simplest exactly solvable quantum model is the zero-range potential (ZRP) model, in which it is possible to obtain the exact quasistationary, quasienergy state (QQES) or Floquet wave function of a weakly bound electron in a strong laser field [5]. (For some applications of the ZRP model to strong field processes, see the reviews [6,7].) As discussed in Ref. [4], the use of ZRP or finite-range potential wave functions gives unexpectedly good qualitative agreement with experimental results for strong field plateau features (with quantitative differences corresponding mainly to the height of such plateaus, which may be attributed to Coulomb effects). HHG calculations employing the ZRP QQES wave function were presented in Refs. [8–15]. TDER theory represents the next-level analytical model in intense laser-atom physics. It contains the ZRP model as a special limiting case and generalizes the ZRP model to the case of an electron with nonzero angular momentum that is bound in a short-range potential. Exactly solvable quantum models allow one to clarify some key aspects of the theory of strong field processes [such as the quantum origin of high-energy (rescattering) plateaus in terms of the exact wave function of an initially bound electron subjected to a strong laser field [15]] and also allow one to justify the use of the length gauge for the laser-atom interaction in approximate (gauge-dependent) analyses [2,15,16] (see also Refs. [17,18]). In addition, TDER theory provides quantitatively accurate predictions for strong-field effects involving negative ions having *s* and *p* state outer (weakly bound) electrons (see, e.g., a recent finite-range potential Floquet-Sturmian treatment of above-threshold detachment for H^- and F^- ions in Ref. [19], the results of which agree with ZRP and TDER theory results).

This paper is organized as follows. In Sec. II we apply the formulation of the HHG amplitude in terms of a system's complex quasienergy to TDER theory [2,3] in order to extend the latter theory to the description of HHG. In Sec. III we examine various approximations to the exact TDER HHG amplitudes. In Sec. IV we present numerical results of TDER theory for HHG by various negative ions, examining the role of initial state symmetry on HHG spectra. We also compare our exact TDER theory results with those of more approximate approaches. In Sec. V we consider the scaling of our results for negative ions to the case of neutral atom targets. In Sec. VI we summarize the key results of this paper and present some conclusions. Some complicated analytical formulas and their mathematical derivations are presented in two Appendixes.

II. HARMONIC GENERATION AMPLITUDE IN TDER THEORY

A. TDER theory for a bichromatic field with commensurate frequencies

We use the quasienergy (or Floquet) approach to treat the electric-dipole interaction, $V(\mathbf{r},t)$, of a strong monochro-

matic laser pulse with a bound electron, whose complex quasienergy, ϵ, and QQES wave function, $\Phi_\epsilon(\mathbf{r},t)$, satisfy the following eigenvalue equation [cf. Eq. (7) in paper I],

$$\hat{\mathcal{H}}(\mathbf{r},t)\Phi_\epsilon(\mathbf{r},t) = \epsilon\Phi_\epsilon(\mathbf{r},t),$$

$$\hat{\mathcal{H}}(\mathbf{r},t) \equiv -\frac{\hbar^2}{2m}\nabla^2 + U(\mathbf{r}) + V(\mathbf{r},t) - i\hbar\frac{\partial}{\partial t}. \tag{1}$$

Here $U(\mathbf{r})$ is a short-range potential confined to the sphere, $r<r_c$. It supports a shallow bound state, $\psi_0(\mathbf{r}) = \varphi_{\kappa lm}(r)Y_{lm}(\hat{\mathbf{r}})$, having energy $E_0=-(\hbar\kappa)^2/(2m)$ $(\kappa r_c \ll 1)$ and angular momentum l. For this case, the complex quasienergy, ϵ, corresponding to the unperturbed energy, E_0, as well as the analytical solution of Eq. (1) for $\Phi_\epsilon(\mathbf{r},t)$ for $r>r_c$ can be obtained within the framework of TDER theory [2]. In brief, the effective range theory represents a generalization of the ZRP model [20] in two main ways. First, in addition to the binding energy $|E_0|$, which is the only parameter within the ZRP model, it introduces a second parameter, the coefficient $C_{\kappa l}$ of the known asymptotic form of $\varphi_{\kappa lm}(r)$ for a finite-range potential $U(r)$,

$$\varphi_{\kappa lm}(r \gg \kappa^{-1}) \approx C_{\kappa l} r^{-1}\exp(-\kappa r), \tag{2}$$

thus providing a more precise, two-parameter description of atomic systems having a valence electron in a bound s state. Second, the effective range theory allows one to extend a ZRP-like analysis to weakly bound valence electron states having nonzero angular momentum, l. Note that the parameters $|E_0|$ and $C_{\kappa l}$ are simply related to the usual parameters of effective range theory for low-energy collisions, the scattering length, a_l, and the effective range, r_l. The correspondence between the two pairs of parameters, $\{a_l, r_l\}$ and $\{\kappa, C_{\kappa l}\}$, is given by the following relations [21,22]:

$$2\kappa C_{\kappa l}^{-2} + r_l\kappa^{1-2l} = (-1)^l(2l+1),$$

$$a_l^{-1} + r_l\kappa^2/2 = (-1)^l\kappa^{2l+1}. \tag{3}$$

Our extension of effective range theory to time-dependent, QQES problems is based on known applications of this theory to time-independent problems involving the analysis of quasistationary (or resonance) states of a weakly bound particle having nonzero l [22,23].

For distances $r>r_c$ (i.e., outside the atomic core potential), the QQES wave function, $\Phi_\epsilon(\mathbf{r},t)$, in TDER theory is expressed in terms of the Volkov Green function $G^{(V)}$ [for which we use the known Feynman form in terms of the classical action; see, e.g., Eqs. (A3)–(A5) in paper I] [15]:

$$\Phi_\epsilon(\mathbf{r},t) = -\frac{2\pi\hbar^2}{m}\lim_{\mathbf{r}'=0}\mathcal{Y}_{lm}(\nabla_{\mathbf{r}'}) \times \int_{-\infty}^{t} G^{(V)}(\mathbf{r},t;\mathbf{r}',t')f_\epsilon(t')e^{i\epsilon(t-t')/\hbar}dt', \tag{4}$$

where $\mathcal{Y}_{lm}(\nabla_{\mathbf{r}'})$ is a differential operator having the form of a solid harmonic, $\mathcal{Y}_{lm}(\mathbf{r}) \equiv r^l Y_{lm}(\hat{\mathbf{r}})$, with the substitution $\mathbf{r} \to \nabla_{\mathbf{r}}$ [e.g., for $l=1$: $\mathcal{Y}_{10}(\nabla_{\mathbf{r}}) = \sqrt{3/(4\pi)}\partial/\partial z$, $\mathcal{Y}_{1,\pm1}(\nabla_{\mathbf{r}}) = \mp\sqrt{3/(8\pi)}(\partial/\partial x \pm i\partial/\partial y)$; for the explicit form of $\Phi_\epsilon(\mathbf{r},t)$ in Eq. (4) for s and p states, see Ref. [3]]. The periodic function $f_\epsilon(t)$ $[f_\epsilon(t)=\Sigma_k f_k \exp(-i2k\omega t)]$ satisfies a one-dimensional eigenvalue equation for ϵ [cf. Eqs. (8) and (9) below], which follows from matching $\Phi_\epsilon(\mathbf{r},t)$ in Eq. (4) to the boundary condition for $\Phi_\epsilon(\mathbf{r},t)$ at small r, $r_c<r\ll\kappa^{-1}$ [which is thus independent of the shape of $U(\mathbf{r})$],

$$\Phi_\epsilon(\mathbf{r},t) = \sum_s \Phi_s(\mathbf{r})e^{-is\omega t} = Y_{lm}(\hat{\mathbf{r}})\sum_k [r^{-l-1} + \cdots + B_l(\epsilon + 2k\hbar\omega) \times (r^l + \cdots)]f_k e^{-i2k\omega t}, \tag{5}$$

where the coefficient $B_l(\epsilon+2k\hbar\omega)$ is related to the effective range parameters by [24]

$$(2l-1)!!(2l+1)!!B_l(\epsilon+2k\hbar\omega) = -1/a_l + r_l\bar{k}^2/2,$$

$$\bar{k}^2 = 2m(\epsilon+2k\hbar\omega)/\hbar^2. \tag{6}$$

Although the TDER approach was formulated originally in Ref. [2] for a monochromatic field, $\mathbf{F}(t) = F\,\mathrm{Re}[\mathbf{e}\exp(-i\omega t)]$ $(\mathbf{e}\cdot\mathbf{e}^*=1)$, the basic equations of TDER theory, (4) and (5), are valid also for the more general case of a multifrequency field with commensurable frequencies $(\omega, 2\omega, \ldots)$ provided that $G^{(V)}(\mathbf{r},t;\mathbf{r}',t')$ in Eq. (4) is the Green function for a free electron in the multicolor field. We consider below the case of a two-color, linearly polarized field,

$$V(\mathbf{r},t) = -\mathbf{d}\cdot\tilde{\mathbf{F}}(t), \quad \mathbf{d} = e\mathbf{r}, \quad \tilde{\mathbf{F}}(t) = \mathbf{e}_z\tilde{F}(t),$$

$$\tilde{F}(t) = F\cos\omega t + F_h\cos\Omega t, \quad \Omega = N\omega, \tag{7}$$

which is appropriate for the analysis of both the HHG amplitude $(\mathcal{A}_N^{(|m|)})$ and the HHG rate $(\mathcal{R}_N)$ (for details, see Sec. III in paper I).

A key advantage of the TDER approach is that it reduces the four-dimensional eigenvalue equation (1) to a one-dimensional, integro-differential equation for $f_\epsilon(t)$ and ϵ. The explicit form of this equation depends on the spatial symmetry of the initial state $\psi_0(\mathbf{r})$. For an s state $\psi_0(\mathbf{r})$, it has the following form [cf. Ref. [15] for the case $\tilde{\mathbf{F}}(t)=\mathbf{F}(t)$]:

$$\left(|E_0| + \frac{\kappa r_0}{2}(\tilde{\epsilon}-E_0)\right)\tilde{f}_{\tilde{\epsilon}}(t) + i\hbar\frac{\kappa r_0}{2}\frac{d\tilde{f}_{\tilde{\epsilon}}(t)}{dt} = \sqrt{\frac{\hbar|E_0|}{4\pi i}}\int_0^\infty \frac{d\tau}{\tau^{3/2}}[e^{(i/\hbar)[\tilde{\epsilon}\tau+S(t,t-\tau)]}\tilde{f}_{\tilde{\epsilon}}(t-\tau) - \tilde{f}_{\tilde{\epsilon}}(t)], \tag{8}$$

where $S(t,t-\tau)\equiv S(\mathbf{r}=0,t;\mathbf{r}'=0,t-\tau)$ is the classical action for an electron in the field $\widetilde{\mathbf{F}}(t)$. [The tilde symbol over a quantity a, i.e., $\tilde{a}$, marks quantities corresponding to the two-color field $\widetilde{\mathbf{F}}(t)$.] For a p-state $\psi_0(\mathbf{r})$, the equation for $\tilde{f}^{(m)}_{\tilde{\epsilon}}(t)$ is more complicated, both because of the differentiations in Eq. (4) and also because of its dependence on the magnetic quantum number, $m=0,\pm 1$, of the QQES $\Phi_{\epsilon_{|m|},m}(\mathbf{r},t)$ being considered,

$$\left(|E_0|+\frac{r_1}{2\kappa}(\tilde{\epsilon}-E_0)\right)\tilde{f}^{(m)}_{\tilde{\epsilon}}(t)+i\hbar\frac{r_1}{2\kappa}\frac{d\tilde{f}^{(m)}_{\tilde{\epsilon}}(t)}{dt}=-\frac{3}{4}\sqrt{\frac{i\hbar^3}{\pi|E_0|}}\{L[\tilde{f}^{(m)}_{\tilde{\epsilon}}(t)]+i\delta_{m,0}\mathcal{L}[\tilde{f}^{(m)}_{\tilde{\epsilon}}(t)]\}, \tag{9}$$

where the integral terms $L[\tilde{f}^{(m)}_{\tilde{\epsilon}}(t)]$ and $\mathcal{L}[\tilde{f}^{(m)}_{\tilde{\epsilon}}(t)]$ are

$$L[f(t)]=\int_0^\infty \frac{e^{(i/\hbar)[\tilde{\epsilon}\tau+iS(0,t;0,t-\tau)]}f(t-\tau)-[1+(i/\hbar)\tilde{\epsilon}\tau]f(t)+\tau df(t)/dt}{\tau^{5/2}}d\tau, \tag{10}$$

$$\mathcal{L}[f(t)]=\frac{e^2}{m\hbar}\int_0^\infty \frac{e^{(i/\hbar)[\tilde{\epsilon}\tau+iS(0,t;0,t-\tau)]}}{\tau^{3/2}}\left(\frac{\mathcal{R}(t)-\mathcal{R}(t-\tau)}{\tau}-\frac{d\mathcal{R}(t-\tau)}{dt}\right)\left(\frac{\mathcal{R}(t)-\mathcal{R}(t-\tau)}{\tau}-\frac{d\mathcal{R}(t)}{dt}\right)f(t-\tau)d\tau,$$

$$\mathcal{R}(t)=\frac{F\cos(\omega t)}{\omega^2}+\frac{F_h\cos(\Omega t)}{\Omega^2}. \tag{11}$$

For practical calculations of the complex quasienergy $\tilde{\epsilon}_{|m|}$, it is convenient to rewrite the eigenvalue integro-differential equations (8) and (9) in an alternative form: as an infinite system of linear homogeneous equations for the Fourier coefficients, $\tilde{f}_k$, of $\tilde{f}_{\tilde{\epsilon}}(t)$. [For the case of a p state $\psi_0(\mathbf{r})$ and a monochromatic field $\mathbf{F}(t)=\mathbf{e}_z F\cos\omega t$, these matrix equations can be found in Ref. [2]; see also Eq. (20) below.] The system of matrix equations for $\tilde{f}_k$ and $\tilde{\epsilon}_{|m|}$ for both s and p states may be written in the following form:

$$\sum_{k'}\tilde{\mathcal{M}}^{(m)}_{k,k'}(\tilde{\epsilon}_{|m|})\tilde{f}^{(m)}_{k'}=0, \tag{12}$$

where

$$\tilde{\mathcal{M}}^{(m)}_{k,k'}(\tilde{\epsilon})=\tilde{M}^{(m)}_{k,k'}(\tilde{\epsilon})-\mathcal{R}_l(\tilde{\epsilon}+2k\omega)\delta_{k,k'}, \tag{13}$$

$$\mathcal{R}_l(\tilde{\epsilon}+2k\omega)=(-\tilde{\epsilon}-2k\omega)^{1/2+l}-1+(-1)^l\frac{r_l}{2}(1+\tilde{\epsilon}+2k\omega), \tag{14}$$

and where the subscript l in $\mathcal{R}_l$ is equal to 0 (1) for an s (p) state $\psi_0(\mathbf{r})$. The matrix elements $\tilde{M}^{(m)}_{k,k'}(\tilde{\epsilon}_{|m|})$ may be expressed explicitly in terms of one-dimensional integrals involving Bessel functions. Note that while we do not present these general expressions for the bichromatic field case here, we do present in Appendix A results for the case $F_h=0$, $\tilde{M}^{(m)}_{k,k'}(F_h=0)\equiv M^{(m)}_{k,k'}$, which turn out to be the ones required in our HHG calculations.

In Eqs. (12)–(14) as well as in the rest of this paper we use the following scaled units (unless otherwise indicated): The field amplitudes are measured in units of $F_0=\sqrt{2m|E_0|}^3/(e\hbar)$; energies and $\hbar\omega$ in units of $|E_0|$, and lengths in units of κ^{-1}, where $\kappa=\sqrt{2m|E_0|}/\hbar$.

B. TDER theory formulation for the HHG amplitude

The TDER theory Eqs. (8)–(14) are quite general and allow for a nonperturbative treatment of both the laser and harmonic fields. For calculations of both the HHG amplitude, $\mathcal{A}_N^{(|m|)}$, and the HHG rate, $\mathcal{R}_N$ (in scaled units), we use the following basic equations in terms of the complex quasienergy (cf. Secs. III and V in paper I):

$$\tilde{\mathbf{d}}^{(|m|)}_{N\omega}=-4\frac{\partial\Delta\epsilon_{|m|}}{\partial\mathbf{F}_h^*}=\tilde{\chi}_N^{(|m|)}(\omega,F)\mathbf{e}_z, \tag{15}$$

$$\mathcal{A}_N^{(|m|)}=\mathbf{e}'^*\cdot\tilde{\mathbf{d}}^{(|m|)}_{N\omega}=\tilde{\chi}_N^{(|m|)}(\omega,F)(\mathbf{e}'^*\cdot\mathbf{e}_z), \tag{16}$$

$$\mathcal{R}_N=\frac{(\alpha N\omega)^3}{8\pi}\frac{1}{2l+1}\sum_m|\tilde{\chi}_N^{(|m|)}(\omega,F)|^2, \tag{17}$$

where $\alpha=1/137$, $\Delta\epsilon_{|m|}$ is the linear in F_h correction to the complex quasienergy $\epsilon_{|m|}$ in a strong linearly polarized laser field $\mathbf{F}(t)$, $\tilde{\mathbf{d}}^{(|m|)}_{N\omega}$ is the Fourier component of the dual dipole moment $\tilde{\mathbf{d}}(t)$ for the harmonic frequency $\Omega=N\omega$, and $\tilde{\chi}_N^{(|m|)}(\omega,F)$ is the generalized nonlinear susceptibility.

To obtain an explicit expression for $\Delta\epsilon_{|m|}$, we expand the matrix elements $\tilde{\mathcal{M}}^{(m)}_{k,k'}(\tilde{\epsilon}_{|m|})$ in Eq. (12) in a series in F_h (up to terms linear in F_h) and in the small parameter $\Delta\epsilon_{|m|}\sim F_h$: $\Delta\epsilon_{|m|}=\tilde{\epsilon}_{|m|}-\epsilon_{|m|}$, where $\epsilon_{|m|}$ is the complex quasienergy at $F_h=0$, i.e., in the laser field $\mathbf{F}(t)$. The system of matrix equations (12) may then be written as follows:

TABLE I. Normalization factor $(-1)^l\mathcal{N}_{|m|}$ [cf. Eq. (23)] for H^- and F^- for three values of F and ω. Note that $(n)\equiv 10^n$.

Ion	$\omega=0.098$ $F=0.1$	$\omega=0.203$ $F=0.3$	$\omega=0.456$ $F=0.6$
H^-[a]	$5.319-i7.724(-6)$	$5.263-i7.479(-3)$	$5.204+i1.496(-1)$
$F^-(m=0)$[b]	$1.410-i1.082(-4)$	$1.397-i7.295(-3)$	$1.375+i2.591(-2)$
$F^-(\lvert m\rvert=1)$[b]	$1.410-i3.621(-8)$	$1.410-i3.481(-4)$	$1.406+i4.649(-3)$

[a]Field-free value, $\mathcal{N}(F=0)=C_{\kappa 0}^2=5.308$ [25].
[b]Field-free value, $-\mathcal{N}(F=0)=C_{\kappa 1}^2=1.411$ [26].

$$\sum_{k'}\left(\mathcal{M}_{k,k'}^{(m)}(\epsilon_{|m|})+\Delta\epsilon_{|m|}\frac{d}{d\tilde{\epsilon}}\mathcal{M}_{k,k'}^{(m)}(\tilde{\epsilon})\Big|_{\tilde{\epsilon}=\epsilon_{|m|}}+\frac{F_h}{4}[d_{N;k,k'}^{(m)}(\epsilon_{|m|})+d_{-N;k,k'}^{(m)}(\epsilon_{|m|})]\right)\tilde{f}_{k'}^{(m)}=0, \tag{18}$$

where

$$\mathcal{M}_{k,k'}^{(m)}(\tilde{\epsilon})=M_{k,k'}^{(m)}(\tilde{\epsilon})-\mathcal{R}_l(\tilde{\epsilon}+2k\omega)\delta_{k,k'}. \tag{19}$$

Explicit forms for the matrix elements $M_{k,k'}^{(m)}(\tilde{\epsilon})$ and $d_{\pm N;k,k'}^{(m)}(\epsilon_{|m|})$ in terms of one-dimensional integrals involving Bessel functions are given in Appendix A.

In order to obtain $\Delta\epsilon_{|m|}$ to lowest nonvanishing order in F_h, we first multiply Eq. (18) by $\tilde{f}_k^{(m)}$ and sum over k. (The coefficients $\tilde{f}_k^{(m)}$ are assumed to be normalized by the condition $\tilde{f}_0^{(m)}=1$.) Then we rewrite $\tilde{f}_k^{(m)}$ as $\tilde{f}_k^{(m)}\approx f_k^{(m)}+\Delta f_k^{(m)}$, where $\Delta f_k^{(m)}\sim F_h$, and make use of Eq. (18) for $F_h=0$ [cf. Eq. (12)],

$$\sum_{k'}\mathcal{M}_{k,k'}^{(m)}(\epsilon_{|m|})f_{k'}^{(m)}=0. \tag{20}$$

In this way, one thus obtains

$$\Delta\epsilon_{|m|}=-\frac{F_h}{4}\frac{\sum_{k,k'}f_k^{(m)}(d_{N;k,k'}^{(m)}+d_{-N;k,k'}^{(m)})f_{k'}^{(m)}}{\sum_{k,k'}f_k^{(m)}\left(\frac{d}{d\tilde{\epsilon}}\mathcal{M}_{k,k'}^{(m)}(\tilde{\epsilon})\right)_{\tilde{\epsilon}=\epsilon_{|m|}}f_{k'}^{(m)}}. \tag{21}$$

[Note that terms involving $d_{N;k,k'}^{(m)}(\epsilon_{|m|})$ and $d_{-N;k,k'}^{(m)}(\epsilon_{|m|})$ in this equation correspond to terms involving $\mathbf{e}'^*$ and $\mathbf{e}'$ in Eq. (25) of paper I for $\Delta\epsilon$.]

According to Eq. (15), the nonlinear susceptibility $\tilde{\chi}_N^{(|m|)}(\omega,F)$ is given by the term involving $d_{N;k,k'}^{(m)}$ in Eq. (21),

$$\tilde{\chi}_N^{(|m|)}(\omega,F)=\mathcal{N}_{|m|}\sum_{k,k'}f_k^{(m)}d_{N;k,k'}^{(m)}(\epsilon_{|m|})f_{k'}^{(m)}, \tag{22}$$

where $\mathcal{N}_{|m|}$ is a dimensionless "normalization factor,"

$$(\mathcal{N}_{|m|})^{-1}=\sum_{k,k'}f_k^{(m)}f_{k'}^{(m)}\left(\frac{d}{d\tilde{\epsilon}}\mathcal{M}_{k,k'}^{(m)}(\tilde{\epsilon})\right)_{\tilde{\epsilon}=\epsilon_{|m|}}. \tag{23}$$

Then $\mathcal{A}_N^{|m|}$ and $\mathcal{R}_N$ may be calculated using Eqs. (16) and (17), respectively. Note that for zero laser field, we have $f_k^{(m)}=\delta_{k,0}$, $\mathcal{M}_{0,0}^{(m)}(\tilde{\epsilon})\to-\mathcal{R}_l(\tilde{\epsilon})$, and $\epsilon_{|m|}=E_0=-1$, so that the field-free value of the normalization factor equals $[\mathcal{N}(F=0)]^{-1}=[2l+1-(-1)^l r_l]/2$ or, in absolute units, $[\mathcal{N}(F=0)]^{-1}=[2l+1-(-1)^l r_l\kappa^{1-2l}]/2$. According to Eq. (3), $\mathcal{N}(F=0)$ is simply related to the asymptotic coefficient in Eq. (2): $\mathcal{N}(F=0)=(-1)^l C_{\kappa l}^2\kappa^{-1}$ [$=(-1)^l C_{\kappa l}^2$, in scaled units]. As shown in Table I for H^- ($|E_0|=0.755$ eV, $C_{\kappa 0}=2.304$ [25]) and F^- ($|E_0|=3.4$ eV, $C_{\kappa 1}=1.188$ [26]), the numerical values of $\mathcal{N}_{|m|}$ for $\omega<1, F<1$ differ only slightly from $\mathcal{N}(F=0)$.

In our derivations of $\Delta\epsilon_{|m|}$ and $\tilde{\chi}_N^{(|m|)}(\omega,F)$ in Eqs. (21) and (22) we have not used the concept of dual QQES wave functions $\tilde{\Phi}_\epsilon(\mathbf{r},t)$ [cf. Eqs. (13) and (14) in paper I] at all, but instead have employed only the exact equations (8) and (9) for the complex quasienergy within TDER theory. As discussed above, our motivation was to derive HHG rates without the necessity of knowing the system's wave function over all space. However, for s states, the QQES wave function (4) is indeed valid over the whole space, $0<r<\infty$, and, at zero effective range, $r_0=0$, coincides with that for the ZRP model [2] upon substituting $C_{\kappa l}=\sqrt{2}$ ($C_{\kappa l}=\sqrt{2\kappa}$ in absolute units). This wave function may thus be normalized by the procedure described in detail in paper I [cf. Eqs. (13) and (14) in paper I] (for a similar treatment for the ZRP model, see Refs. [6,7]). Consequently, it may be used for direct calculations of the dual dipole moment, $\tilde{\mathbf{d}}(t)=\langle\tilde{\Phi}_\epsilon(t)|\mathbf{d}|\Phi_\epsilon(t)\rangle$, and its Fourier components $\tilde{\mathbf{d}}_{N\omega}$ [cf. Eqs. (15) and (16) in paper I] in terms of $\Phi_\epsilon(\mathbf{r},t)$ and $\tilde{\Phi}_\epsilon(\mathbf{r},t)$. We do not present these alternative derivations here, but emphasize that the result coincides exactly with that in Eq. (22) for an s state $\psi_0(\mathbf{r})$ and also, for $r_0=0$, with the result for a ZRP model, presented in the Appendix of paper I, which is obtained by direct calculation of the matrix element $\langle\tilde{\Phi}_\epsilon(t)|\mathbf{d}|\Phi_\epsilon(t)\rangle$. This self-consistency provides strong justification for using the dual dipole moment to correctly define the HHG amplitude for a nonstable atomic system.

III. APPROXIMATE VERSIONS OF THE TDER THEORY HHG AMPLITUDE

We analyze here how some common approximate treatments for the HHG amplitude may be obtained as approxi-

mations to the exact TDER theory HHG amplitude formulated in Sec. II B. We first consider an approximation equivalent to that in the well-known Keldysh theory for the ionization amplitude [27,28], i.e., replacing the final state in the exact result for the ionization amplitude by a Volkov wave function. We then analyze semiclassical approximations to the Keldysh approximation (KA) result for the HHG amplitude, similarly to the quasiclassical (low frequency, or stationary phase) analyses of the KA ionization amplitude in the tunneling limit.

A. Keldysh approximation for HHG in TDER theory

In order to obtain both an approximate TDER result for the HHG amplitude and also an interpretation of the exact expression (22), we note that, as shown in Eq. (5), the coefficients f_k determine the "population" of Floquet (or QES) harmonics, $\Phi_s(\mathbf{r})$, of the QQES wave function,

$$\Psi_\epsilon(\mathbf{r},t) = e^{-i\epsilon t}\Phi_\epsilon(\mathbf{r},t) = \sum_s \Phi_s(\mathbf{r})e^{-i(\epsilon+s\omega)t}, \tag{24}$$

near the origin, where only even ($s=2k$) QES harmonics are nonzero [15]. Moreover, in terms of these coefficients, the exact wave function $\Phi_\epsilon(\mathbf{r},t)$ in Eq. (4) at $r>r_c$ may be represented [in a form alternative to (24)] as a sum of quasienergy "KA harmonics," $\Phi^{\mathrm{KH}}_{\epsilon+2k\omega}(\mathbf{r},t)$ (cf. Ref. [15]),

$$\Phi_\epsilon(\mathbf{r},t) = \sum_{k=-\infty}^{\infty} f_k \Phi^{\mathrm{KH}}_{\epsilon+2k\omega}(\mathbf{r},t). \tag{25}$$

(Note the 2ω spacing of the KA harmonics.) The definition of $\Phi^{\mathrm{KH}}_{\epsilon+2k\omega}$ follows straightforwardly from Eq. (4) [and the definition of $f_\epsilon(t)$ just below Eq. (4)]:

$$\Phi^{\mathrm{KH}}_{\epsilon+2k\omega}(\mathbf{r},t) = -2\pi \lim_{\mathbf{r}'=0} \mathcal{Y}_{lm}(\nabla_{\mathbf{r}'}) \int_{-\infty}^{t} G^{(V)}(\mathbf{r},t;\mathbf{r}',t') \times \exp[i\epsilon(t-t') - 2ik\omega t']dt'. \tag{26}$$

The coefficients f_k (or $f^{(m)}_k$, for p states) are key objects of the TDER theory since they contain complete information on high-order binding potential effects (which, as is commonly accepted, are responsible for rescattering effects) during the interaction of an initially bound electron with a laser field [2]. In contrast, the KA harmonics describe the free evolution (of the electron in the laser field) as monochromatic QES harmonics of frequency $2k\omega$ created near the origin as a result of the binding potential-mediated exchange of an even number of photons between the electron and the laser field. As may be seen in Eq. (26), the KA harmonics have a remarkably similar form for different k, differing only in the value of the "energy parameter," $\epsilon+2k\omega$. Thus the terms $f^{(m)}_k d^{(m)}_{N;k,k'} f^{(m)}_{k'}$ with $k,k'\neq 0$ in Eq. (22) describe binding potential-induced contributions to the HHG amplitude $\mathcal{A}^{(|m|)}_N$ that originate from electron transitions between the kth and the k'th KA harmonics. However, both our numerical and analytical investigations in Ref. [15] show that in the low-frequency (tunneling) regime the coherent sum of these contributions in Eq. (22) has only a small effect on the HHG amplitude $\mathcal{A}^{(|m|)}_N$, which is dominated by the $k=k'=0$ term. Approximating $\epsilon_{|m|}$ by $E_0=-1$ and $\mathcal{N}_{|m|}$ by $\mathcal{N}(F=0) = (-1)^l C^2_{\kappa l}$, the term with $k=k'=0$ in Eq. (22) determines the HHG amplitude in the KA,

$$\mathcal{A}^{\mathrm{KA}}_N = (-1)^l C^2_{\kappa l} d^{(m)}_{N;0,0}(\epsilon_{|m|}=E_0)(\mathbf{e}'^{*}\cdot\mathbf{e}_z). \tag{27}$$

The KA HHG amplitude (27) represents a drastic simplification of the exact TDER result [given by Eqs. (16) and (22)] that avoids the most laborious problem in exact TDER calculations: numerical solution of the matrix equation (20) for $\epsilon_{|m|}$ and the Fourier coefficients $f^{(m)}_k$.

Although the KA is usually understood as an approximation for the ionization amplitude [27,28], we use this terminology also in this HHG study because the KA harmonic in Eq. (25) with $k=0$ and $\epsilon=E_0$ corresponds to the QQES TDER wave function $\Phi_\epsilon(\mathbf{r},t)$ in the KA [15]:

$$\Phi_{\mathrm{KA}}(\mathbf{r},t) \equiv \Phi^{\mathrm{KH}}_{\epsilon=E_0}(\mathbf{r},t) = -2\pi \lim_{\mathbf{r}'=0} \mathcal{Y}_{lm}(\nabla_{\mathbf{r}'}) \int_0^{\infty} e^{iE_0 t'} G^{(V)}(\mathbf{r},t;\mathbf{r}',t-t')dt'. \tag{28}$$

The subscript KA is, in turn, used for this wave function since its asymptotic form at large distances yields the "exact" KA result for the ionization amplitude (in terms of generalized Bessel functions; see Refs. [2,15]), which in the quasiclassical limit ($\omega \ll 1$) reduces to known results for tunneling ionization [29–31]. In addition, for $F\to 0$, the large r (asymptotic) form of $\Phi_{\mathrm{KA}}(\mathbf{r},t)$ reduces to the asymptotic form of $\psi_0(\mathbf{r}) = \varphi_{\kappa lm}(r)Y_{lm}(\hat{\mathbf{r}})$ in Eq. (2). Thus the KA wave function (28) accounts for binding potential effects on the same level of accuracy as in the KA for the ionization amplitude [27,28], i.e., only on the level of the initial state wave function $\psi_0(\mathbf{r})$ (cf. Ref. [15] for further discussion). Note finally, that the KA HHG amplitude (27) for the case of an s state $\psi_0(\mathbf{r})$ coincides with both the S-matrix result in Ref. [32] and the "Keldysh-type approximation" of Ref. [33] provided that both these results include terms corresponding to the so-called "continuum-continuum transitions" [34].

B. Quasiclassical results for the KA HHG amplitude

The KA HHG amplitude $\mathcal{A}^{\mathrm{KA}}_N$ in Eq. (27) is determined by the matrix element $d^{(m)}_{N;0,0}(E_0)$, whose analytical expression [for either an s or a p initial state $\psi_0(\mathbf{r})$] contains only one-dimensional integrals involving Bessel functions $J_p(z)$ with integer indices p [cf. Eqs. (A2) and (A9)]. However, these Bessel functions have a complicated argument, $z=z(\phi)$ [cf. Eq. (A3)], so that analytical evaluations of the integrals are difficult. On the other hand, neglect of high-order KA harmonics with $|k|>0$ in Eq. (25) is equivalent to the approximation $f_\epsilon(t)\approx$ constant, which is generally valid for low frequencies [5], and thus permits the use of quasiclassical methods to evaluate $d^{(m)}_{N;0,0}(E_0)$. The quasiclassical approximation is appropriate (and very common) for analyses of laser-atom processes in not too strong, low-frequency fields. It usually utilizes the stationary phase method to evaluate

some temporal integrals (see, e.g., Ref. [4]). For both s and p-states of the bound electron, the most profound quasiclassical analysis of the HHG process was performed in Refs. [33,35–38].

For comparison with previous quasiclassical studies and to check the accuracy of the quasiclassical approximation to our "exact" KA result (27) for the HHG amplitude, we present here an alternative derivation of $\mathcal{A}_N^{\mathrm{KA}}$, employing different mathematical techniques from those used in Sec. II B. Instead of the Feynman representation, our derivation employs the "quasienergy form" for the time-dependent Green function $G^{(V)}$ in Eq. (4) (cf. Appendix B). This form allows one to perform some temporal integrations by means of the stationary phase method.

We follow the procedure used for the derivation of $\Delta\epsilon_{|m|}$ in Eq. (21). First, we construct the KA-like wave function, $\Phi_{\tilde{\epsilon}}^{\mathrm{KA}}(\mathbf{r},t)$ (valid in the domain $r>r_c$), for the bichromatic field $\tilde{\mathbf{F}}(t)$ in Eq. (7) by substituting $f_{\tilde{\epsilon}}(t)\to 1$ into Eq. (4) and keeping $\tilde{\epsilon}$ in the exponential, $\exp[i\tilde{\epsilon}(t-t')/\hbar]$, as an unknown parameter. Then, in order to obtain an approximate, low-frequency result for the quasienergy $\tilde{\epsilon}_{|m|}$, we match the time-averaged (over the laser period, T) projection of the function $\Phi_{\tilde{\epsilon}}^{\mathrm{KA}}(\mathbf{r},t)$ onto the spherical harmonics $Y_{lm}(\hat{r})$ by using boundary condition (5) with $f_k=\delta_{k0}$ (cf. Ref. [5]). The result is a transcendental equation for $\tilde{\epsilon}_{|m|}$, whose perturbative (lowest order, i.e., linear in F_h) solution for $\Delta\epsilon_{|m|}=\tilde{\epsilon}_{|m|}-\epsilon_{|m|}$ allows one to obtain the quasiclassical KA result for $\tilde{\mathbf{d}}_{N\omega}^{(|m|)}$ in Eq. (15). As details of the derivations are given in Appendix B, we present here only the final results. The quasiclassical HHG amplitude for an initial s state $\psi_0(\mathbf{r})$ is

$$A_N^{(s)}=2i\sum_s \mathcal{Z}_{0,s}\int_0^T \frac{e^{i[\Omega t+S_s(t_0')-S_s(t)]}(\mathbf{k}_t-\mathbf{K}_s)\cdot\mathbf{e}'^*}{[\cos(\omega t)-\cos(\omega t_0')][(\mathbf{K}_s-\mathbf{k}_t)^2+1]^2}dt. \tag{29}$$

Those for an initial p state $\psi_0(\mathbf{r})$ are

$$A_N^{(p,|m|=1)}=\frac{\omega^2}{F}\sum_s \mathcal{Z}_{1,s}k_s\int_0^T \frac{e^{i[\Omega t+S_s(t_0')-S_s(t)]}(\mathbf{k}_t-\mathbf{K}_s)\cdot\mathbf{e}'^*}{[\cos(\omega t)-\cos(\omega t_0')]^2[(\mathbf{K}_s-\mathbf{k}_t)^2+1]^2}dt, \tag{30}$$

$$A_N^{(p,m=0)}=\sum_s \mathcal{Z}_{1,s}\int_0^T \frac{e^{i[\Omega t+S_s(t_0')-S_s(t)]}[(\mathbf{K}_s-\mathbf{k}_t)^2-1](\mathbf{K}_s-\mathbf{k}_{t_0'})\cdot\mathbf{e}'^*}{[\cos(\omega t)-\cos(\omega t_0')][(\mathbf{K}_s-\mathbf{k}_t)^2+1]^2}dt. \tag{31}$$

In Eqs. (29)–(31) the sum Σ_s is over all open s-photon ATI channels [i.e., those with $s>(u_p+1)/\omega$]; $k_s=\sqrt{s\omega-1-u_p}$ is the photoelectron momentum in the sth channel,

$$S_s(t)=\int^t [\ (\mathbf{K}_s-\mathbf{k}_\tau))^2+1]d\tau,$$

$$\mathbf{K}_s=k_s\frac{\mathbf{F}(t)-\mathbf{F}(t')}{|\mathbf{F}(t)-\mathbf{F}(t')|}=\pm k_s\mathbf{e}_z,\quad \mathbf{k}_t=-\mathbf{e}_z\frac{F}{\omega}\sin\omega t;$$

t_0' is the (complex) stationary point of the function $S_s(t')$ having $\mathrm{Im}\, t_0'>0$ and the smallest real part (see Appendix B); and the "normalization parameter" $\mathcal{Z}_{l,s}$ is

$$\mathcal{Z}_{l,s}=\frac{(2l+1)C_{\kappa l}^2\omega^4}{2\pi^2F}\sqrt{\frac{2\pi i}{S''_s(t_0')}}.$$

Since $(\mathbf{k}_t-\mathbf{K}_s)=\mathbf{e}_z[(F/\omega)\sin\omega t\pm k_s]$, the HHG amplitudes (29)–(31) may also be written similarly to Eq. (16), with obvious definitions for the quasiclassical susceptibilities $\tilde{\chi}_{N\omega}^{(|m|)}(\omega,F)$.

Postponing quantitative comparisons to Sec. IV, we conclude this section with some qualitative remarks concerning comparisons of HHG rates obtained using our quasiclassical results (29)–(31) with those using their more exact KA counterpart (27) as well as with those in the quasiclassical three-step HHG model [33,37,38].

(i) Our quasiclassical HHG rates for both s and p states are in good quantitative agreement with the KA results obtained from Eq. (27) except in two cases: (a) for low harmonics, $\hbar\Omega<|E_0|$, before the plateau onset, and (b) for high frequencies, $\hbar\omega<|E_0|$, in which case the use of stationary phase methods is unjustified.

(ii) For s states, our HHG amplitude (29) coincides exactly with that of Ref. [33].

(iii) For p states, our results using Eqs. (30) and (31) differ from those in Ref. [33]. This discrepancy stems from the use in Ref. [33] of the asymptotic form (2) to approximate $\psi_0(\mathbf{r})$ over the whole space when calculating its Fourier transform, $\tilde{\psi}_0(\mathbf{q})$ $(\mathbf{q}=\mathbf{k}_t-\mathbf{K}_s)$. In contrast, our formulation in Sec. II B is independent of the small-r behavior of $\psi_0(\mathbf{r})$ and $\Phi_\epsilon(\mathbf{r},t)$ beyond the boundary condition (4), which is independent of the shape of $U(\mathbf{r})$. Agreement of the results for s states is not surprising since for this case the asymptotic form (2) determines the whole-space wave function of the bound state of the ZRP model [20], so that $\tilde{\psi}_0(\mathbf{q})$ is valid for any $|\mathbf{q}|$. However, differences between the results in Ref. [37] and those using Eqs. (30) and (31) are to be expected for p-states since the form (2) is incorrect for small r, where

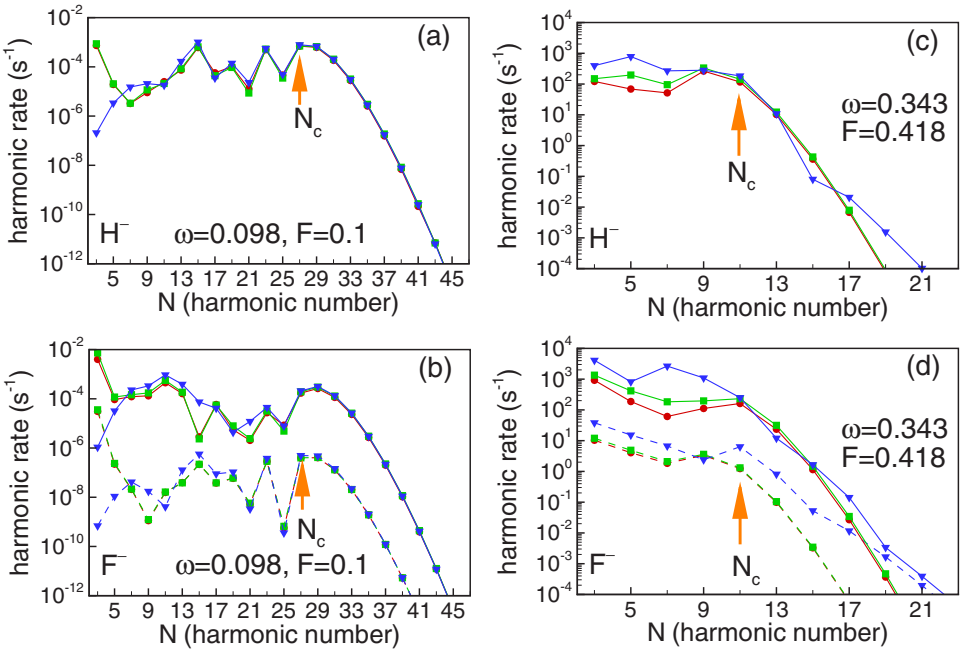

FIG. 1. (Color online) HHG rates for H^- and F^- for low (a),(b) and high (c),(d) frequencies. Results for different approximations are presented: circles (red), exact TDER theory results, Eqs. (17) and (22); squares (green), KA results, Eq. (27); triangles (blue), quasiclassical results [Eq. (29) for H^- and Eqs. (30) and (31) for F^-]. For F^-, the rates for $m=0$ (solid line) and $|m|=1$ (broken line) are presented. Arrows show the positions of the classical cutoffs, $N_c=(|E_0|+3.17u_p)/(\hbar\omega)$, in each case.

$\varphi_{\kappa lm}(r)\sim r^l$. Indeed, this is the case: for $|m|=1$, the result in Ref. [33] is generally divergent [37], whereas, for $m=0$, the result differs significantly from that using Eq. (31), as shown in Sec. IV. In fact, the HHG spectra in Ref. [33] for s and p states differ only by a scaling factor $(\sqrt{3}C_{\kappa 1}/C_{\kappa 0})^4$.

(iv) The sensitivity of p-state HHG rates to the initial state $\psi_0(\mathbf{r})$ is discussed in Ref. [38], where it is shown that use of realistic wave functions gives HHG rates for p states with $m=0$ that are smaller by 1–2 orders of magnitude compared to those in Ref. [37]. The results of Ref. [38] agree reasonably well with our quasiclassical results using Eq. (31).

(v) The factor ω^2/F in Eq. (30) explicitly exhibits the suppression of HHG rates from states with nonzero angular momentum projection m for the case of a strong, low-frequency field, in agreement with the intuitive physical arguments in Ref. [37].

IV. NUMERICAL RESULTS AND DISCUSSION

A. Comparison of different approximations for the HHG amplitude

Our three different results for the HHG amplitude [i.e., the exact TDER theory result in Eqs. (16) and (22); the KA result (27); and the quasiclassical KA results in Eqs. (29)–(31)], enable us to evaluate the accuracy of both the KA and its quasiclassical approximation for HHG calculations. While the KA [i.e., neglect of high-order KA harmonics in Eq. (25)] may be considered as the result to lowest nonvanishing order in the binding potential, the conditions for applicability of the quasiclassical approximation for the HHG amplitude $\mathcal{A}_N$ [33], i.e., $\omega \ll 1$ and $F/\omega^2 \gg 1$ (which are used to evaluate particular integrals), appear to be more restrictive. Since these inequalities are not very specific, it is unclear *a priori* over which range of the parameters ω, F, and N is the accuracy of quasiclassical (or, in fact, stationary phase) methods reasonable. Our comparisons are for the H^- ($|E_0|=0.755$ eV, $C_{\kappa 0}=2.304$ [25]) and F^- ($|E_0|=3.4$ eV, $C_{\kappa 1}=1.188$ [26]) ions, for which there have been experiments [39,40].

For negative ions with ground S states (such as H^- and F^-), we use the following expression for the HHG rate in the single active electron approximation,

$$\tilde{\mathcal{R}}_N = \frac{(\alpha N\omega)^3}{8\pi}\frac{1}{2l+1}\sum_m |\tilde{\chi}_N^{(m)}(\omega,F)|^2, \tag{32}$$

where l is the angular momentum of the outer (weakly bound) electron. The result (32) requires some discussion. Both H^- and halogen negative ions have spherically symmetric ground states (owing to their filled s^2 and p^6 valence shells), so that in an exact *multielectron* formulation the following definition (in absolute units) for the HHG rate in terms of the Fourier component, $\tilde{\mathbf{D}}_{N\omega}$, of a multielectron dual dipole moment $\tilde{\mathbf{D}}(t)$ should be used,

$$\frac{dW_{N\omega,\hat{\mathbf{k}}}}{d\Omega_{\hat{\mathbf{k}}}} \equiv \tilde{\mathcal{R}}_N = \frac{(N\omega)^3}{8\pi\hbar c^3}|\tilde{\mathbf{D}}_{N\omega}|^2. \tag{33}$$

However, for halogen ions in the *single active electron* approximation the definition (32) for $\tilde{\mathcal{R}}_N$ is used, which is similar to that in Eq. (17). Note that the transitions $m \to m' = m \pm 1$ in Eq. (32) are restricted not by the "coherence" condition [as for atoms or ions with nonzero total angular momentum in Eq. (17); cf. Sec. V in paper I], but by the Pauli exclusion principle, as is shown in Ref. [37].

Figures 1(a)–1(d) show, respectively, comparisons for the "low-frequency" ($\omega=0.098, F=0.1$) and "high-frequency" ($\omega=0.343, F=0.418$) HHG spectra for H^- and F^-. (Note that for F^- the frequency $\omega=0.343$ corresponds to Nd:YAG laser radiation, $\lambda=1064$ nm.) In the *low frequency* domain, the KA results are in excellent agreement with the exact ones. [This unprecedented accuracy of the KA in the low-

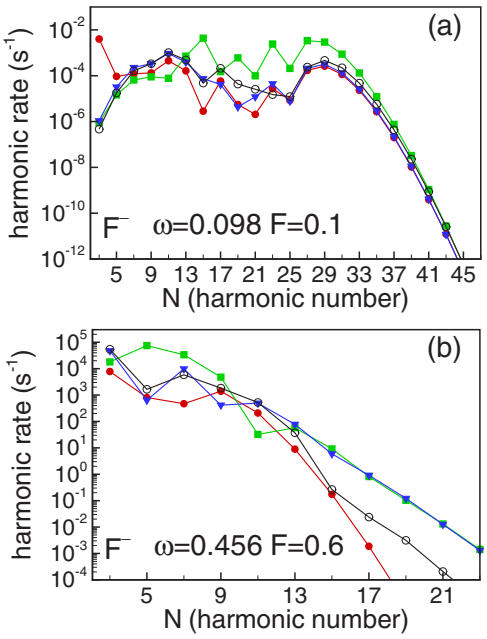

FIG. 2. (Color online) HHG spectrum of F^- for low (a) and high (b) frequencies. Full circles (red), exact TDER results; full squares (green), quasiclassical (three step HHG model [33]) results [37,41]; full triangles (blue), our quasiclassical results [Eq. (31)]; open circles, quasiclassical (three step model) results of Ostrovsky using realistic bound state wave functions [38,41]. Owing to the different definition of HHG rates for halogen ions in Refs. [37,38] as compared to our definition (32), results of Refs. [37,38,41] have been divided by a factor of 3.

frequency, strong-field regime originates from the fact that the HHG amplitude in this regime is described only by *odd* QES harmonics, $\Phi_{N=2k+1}(\mathbf{r})$, of $\Phi_{\epsilon}(\mathbf{r},t)$, which agree well with the KA QES harmonics $\Phi^{\mathrm{KA}}_{N=2k+1}(\mathbf{r})$ over all space, $0<r<\infty$, as shown in Ref. [15].] The quasiclassical results using Eqs. (29)–(31) agree well with the exact ones only around and beyond the classical cutoff. Along the plateau, the latter exhibit deviations from the exact results, especially for *p*-state (F^-) ions. Moreover, the quasiclassical results fail to describe the low-energy part of the HHG spectra, in which the exact HHG rates exhibit perturbativelike (decreasing) behavior with increasing *N*. The results in Figs. 1(a) and 1(b) (as well as our results for other ions) show that for small ω the minimum value of *N* at which the quasiclassical results are reasonable corresponds to the onset of the HHG plateau, i.e., $N>(1/\omega)$ (or $N\geqslant n_0$, where n_0 is the minimum number of photons needed for ionization). In the *high frequency* domain [cf. Figs. 1(c) and 1(d)], the results are quite different. The KA HHG rates overestimate the exact ones along the plateau (except for *p* states with $|m|=1$), but agree with the latter at and beyond the plateau cutoff. The quasiclassical results overestimate the exact ones by an order of magnitude along the plateau and by much more beyond the classical cutoff. Also, the quasiclassical results for $m=0$ and $|m|=1$ [cf. Fig. 1(d)] merge with increasing *N*, in sharp contrast with the KA and exact results.

Figure 2 compares our exact TDER results with results of the three-step HHG model [33], which was used recently to treat negative halogen ions in Refs. [37,38]. As discussed above, use of the asymptotic form (2) for the *p*-state wave function over the whole space leads to incorrect results for $\mathcal{A}_N^{(p,m=0)}$ that differ from those for an *s*-state by only a scaling factor [37]. The use of realistic wave functions [38,41] significantly improves the results in both low [Fig. 2(a)] and high-frequency [Fig. 2(b)] domains, except for the lowest *N* in the former and high *N* (beyond the cutoff) in the latter. Use of realistic initial state wave functions $\psi_0(\mathbf{r})$ [38,41] in the quasiclassical three-step-model calculations of Refs. [37,38] results in much better agreement with our own quasiclassical results (31); however, differences from exact TDER results remain (especially for the low-frequency case). Differences between our exact and quasiclassical results have already been discussed for Fig. 1. In summary, we conclude that regardless of the quality of initial state wave functions, quasiclassical results are generally inaccurate for the low-energy part [$N\leqslant(1/\omega)$] of the HHG spectrum and overestimate HHG rates beyond the cutoff in the high-frequency case.

Finally, we discuss two related questions.

(1) How does the perturbation of the bound state energy E_0 by a laser field (i.e., the Stark shift, Re $\epsilon-E_0$, and the depletion due to photodetachment, described by the level width, $\hbar\Gamma=-2$ Im ϵ) influence the HHG rates?

(2) How do high-order binding potential effects, which are described by the Fourier coefficients $f^{(m)}_{k\neq 0}$, influence the HHG rates in the approximation that $\epsilon=E_0$?

According to our discussion of Figs. 1(a) and 1(b), these effects are negligibly small in the strong-field, low-frequency (tunneling) regime since the exact TDER results are well approximated by the KA ones (in which case $f^{(m)}_k=\delta_{k,0}$ and the complex quasienergy ϵ is approximated by E_0, in particular, because the level width is exponentially small in this regime). To illustrate the situation for a higher frequency regime, in Fig. 3 we compare exact TDER results [obtained using Eqs. (16) and (22)], KA results [given by Eq. (27)], and approximate TDER results corresponding to the case in which both the matrix elements $d^{(m)}_{N;k,k'}(\epsilon_{|m|})$ and the Fourier coefficients $f^{(m)}_k$ in Eq. (22) are calculated for $\epsilon=E_0$. [The coefficients $f^{(m)}_k(\epsilon_{|m|}=E_0)$ are obtained as an approximate solution of the matrix equation (20), i.e., substituting there $\epsilon_{|m|}=E_0$ in the matrix elements $\mathcal{M}^{(m)}_{k,k'}(\epsilon_{|m|})$.] We consider the F^- ion, Nd:YAG laser radiation ($\omega=0.343$), and both "intermediate" [$\xi=u_p/(\hbar\omega)=2.26$; cf. Fig. 3(a)] and strong-field [$\xi=4.52$; cf. Fig. 3(b)] intensity regimes. Comparison of the red (circles) and blue (triangles) curves in Fig. 3 shows that in this high frequency regime ($\hbar\omega\gtrsim 0.3|E_0|$) the influence of the Stark shift and width of the bound state becomes significant for moderate intensities over the entire plateau region, while in the strong field ($\xi\gg 1$) regime the differences are more irregular, but may be considerable in the middle part of the plateau. More important, however, is the second kind of beyond-the-KA correction to the HHG rates obtained by including the coefficients $f^{(m)}_k(\epsilon_{|m|}=E_0)$ that are omitted in the KA. Their effect may be seen in Fig. 3 by comparing the triangles (blue) and squares (green) curves, whose differences are relevant to the rescattering interpretation of plateau

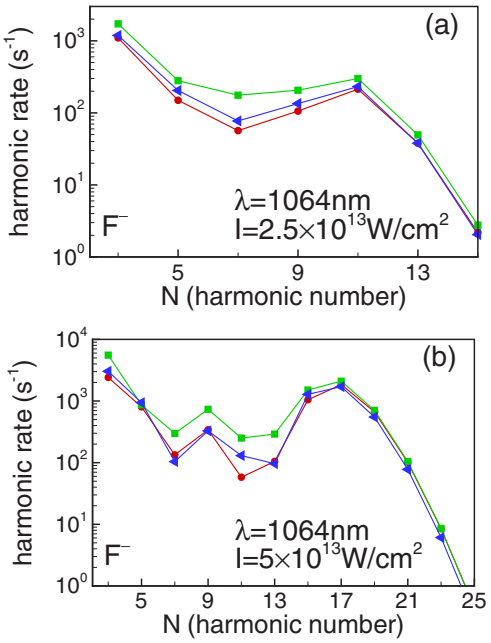

FIG. 3. (Color online) Comparison of exact TDER results [circles (red)], TDER results neglecting the Stark shift of the initial bound state and its width due to photodetachment, i.e., $\epsilon_{|m|}=E_0$ [triangles (blue)], and KA results, i.e., $\epsilon_{|m|}=E_0$, $f_k^{(m)}=\delta_{k,0}$ [squares (green)] for the HHG spectrum of F^- at $\lambda=1064$ nm ($\omega=0.343$) and (a) $I=2.5\times10^{13}$ W/cm^2 ($F=0.427$) and (b) $I=5\times10^{13}$ W/cm^2 ($F=0.604$).

features in HHG processes. Indeed, the remarkable rescattering scenario explanation of plateau features in strong field phenomena (as resulting from repeated interactions of the active electron with the atomic core) was suggested for the first time based on a (quasi)classical description of the HHG process. However, a rigorous quantum analysis in terms of the properties of exact QQES wave functions shows that HHG plateaus in the tunneling regime are well described just by the KA wave function [cf. (28) for the case of TDER theory], which corresponds to a lowest nonvanishing order account of binding potential effects (i.e., on the initial state only), similar to that in the Keldysh theory of tunneling ionization (see Ref. [15] for more details). In contrast, this same analysis shows that only "true rescattering" (i.e., involving higher than lowest order binding potential effects) causes the well-known plateau features in above-threshold ionization/detachment. As mentioned in Sec. III A, high-order binding potential effects in the TDER theory are completely described by the coefficients $f_k^{(m)}$. Therefore, for HHG, such "true rescattering" effects become important only for high (nontunneling) frequencies, and their quantitative measure in the TDER theory is given by the difference between the blue (triangles) and green (squares) curves in Fig. 3, both of which correspond to the same (unperturbed) quasienergy, $\epsilon=E_0$. We observe in Fig. 3 that both approximate results generally overestimate the exact ones, as is typical (usually) of most approximate theories.

B. Initial state symmetry effects

To the best of our knowledge, HHG rates for negative ions with valence p electrons are known for only two ions, F^- and I^-, for one wavelength, $\lambda=800$ nm, i.e., $\omega=0.456$ for F^- and $\omega=0.505$ for I^- [37,38]. We present below a comparative study of HHG rates [obtained using the exact TDER formulas (17) and (22)] for ions with s and p outer electrons for a number of frequencies, from $\omega\approx0.1$ (which is typical for investigations of HHG in rare gas atoms) up to $\omega\approx0.5$. Since ions with s and p outer electrons have rather different binding energies, we present their HHG spectra for the same scaled intensity and photon energy. Moreover, the asymptotic coefficients $C_{\kappa l}$ are also different for s and p states, while the normalization factors $\mathcal{N}_{|m|}$ in Eqs. (22) and (23) are not too sensitive to F and ω (cf. Table I) and remain close to their field-free value, $C_{\kappa l}^2$. Therefore, we introduce the reduced HHG rates,

$$r_N=\tilde{\mathcal{R}}_N C_{\kappa l}^{-4}, \tag{34}$$

where $\tilde{\mathcal{R}}_N$ is the HHG rate in scaled units given by Eq. (32). It is to be expected that differences between reduced rates r_N for s-state and p-state ions for the same scaled F and ω originate entirely from the dependence of harmonic photon emission by these ions on the spatial (s or p) symmetry of the initial state, $\psi_0(\mathbf{r})$, i.e., on the "inner" dynamics. HHG rates in absolute units may be obtained by multiplying r_N by the factor $\mathcal{C}=(|E_0|/\mathcal{E}_a)^2C_{\kappa l}^4\omega_a$, where $\mathcal{E}_a=27.21$ eV and $\omega_a=\mathcal{E}_a/\hbar=4.13\times10^{16}$ s^{-1}. In Table II we present the numerical value of this factor for several ions, although the numerical results for r_n are applicable also for other targets for which the parameters $|E_0|$ and $C_{\kappa l}$ are known. [For the data in Table II, the parameters $|E_0|$ and $C_{\kappa l}$ were taken from Refs. [25] (for H^-) and [26].]

TABLE II. Numerical values of the coefficient $\mathcal{C}=(|E_0|/E_a)^2C_{\kappa l}^4\omega_a$ for several negative ions having s- and p-state outer electrons. $(n)\equiv10^n$.

s state	$\mathcal{C}$ (s^{-1})	p state	$\mathcal{C}$ (s^{-1})
H^-	8.96(14)	O^-	1.98(14)
Li^-	4.65(14)	F^-	1.28(15)
Na^-	4.18(14)	Cl^-	8.85(15)
K^-	2.50(14)	Br^-	1.26(16)
Rb^-	1.51(14)	I^-	3.04(16)

In Fig. 4 we present reduced HHG rates, r_N [cf. Eq. (34)], for ions with s and p outer electrons for four sets of frequency and intensity. For p states, both the total rates and the separate contributions to r_N of the different magnetic sublevels are given. In all cases shown, rates for sublevels with $|m|=1$ are orders of magnitude smaller than for $m=0$, in qualitative agreement with quasiclassical results (30) as well as with physical arguments in Refs. [37,38] based on the three-step HHG mechanism [33]. Nevertheless, the suppression shown in Fig. 4 is much stronger than indicated by the parameter ω^2/F in Eq. (30); this suppression is similar to that for plateau features in above-threshold detachment (ATD) from p states with $|m|=1$ (see Ref. [2], where it is noted that rescattering for this case is suppressed by the centrifugal barrier). Observe also that the *shape* of the $m=\pm1$

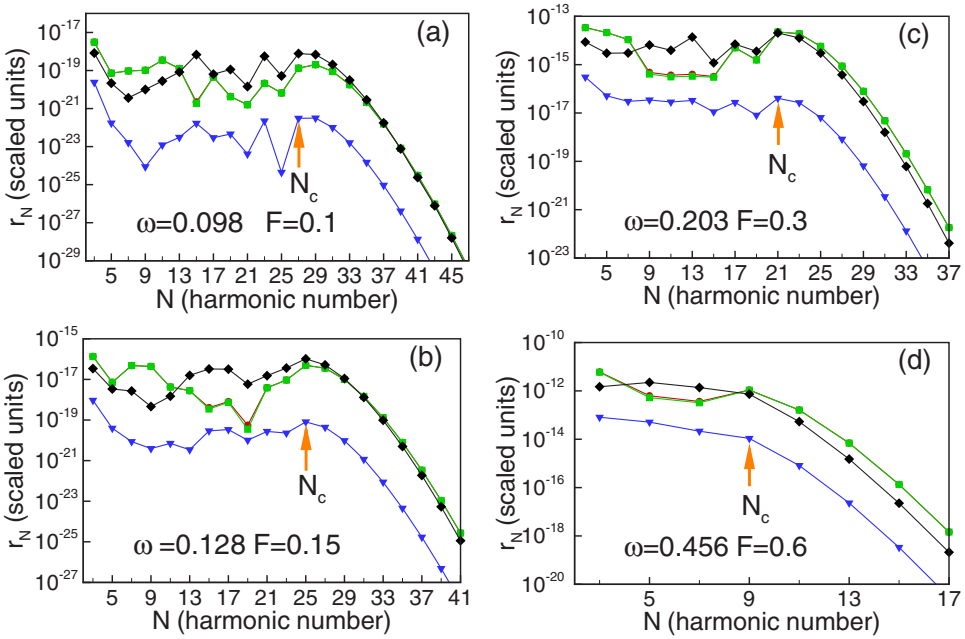

FIG. 4. (Color online) Reduced HHG rates, Eq. (34), for s and p initial states, $\psi_0(\mathbf{r})$. Diamonds (black), s state; circles (red), total harmonic rate for a p state; squares (green), contribution of magnetic sublevel with $m=0$; triangles (blue), contribution of magnetic sublevels with $|m|=1$. Arrows show the positions of the classical cutoffs, $N_c=(|E_0|+3.17u_p)/(\hbar\omega)$. Scaled units are used for ω and F.

rates is qualitatively similar to that for s states [as might be expected owing to the similar structures of the amplitudes (29) and (30)].

Figure 4 shows that, on average, the reduced HHG rates r_N are approximately the same for s and p states; however, with increasing ω, the magnitude of r_N for p states becomes somewhat larger for harmonics beyond the plateau cutoff. Thus, owing to the much greater $\mathcal{C}$ factors for p states (cf. Table II), the absolute harmonic yields for p-state ions are much higher for the same scaled F and ω values. Figure 4 shows also that the oscillation pattern in the HHG rates over the region from the onset up to about the middle of the high-energy plateau are more pronounced for low frequencies and are out of phase for s and p states. These features appear to be general since they occur also in our results for other sets of laser parameters F and ω (not shown here). The low-energy part of the HHG plateau is generally highly irregular and specific to the atomic system and the laser parameters. Indeed, it is not possible to describe this low-energy portion of the HHG plateau in terms of a few classical trajectories or quantum orbits [36,42]. To attain reasonable accuracy using standard stationary phase methods, it is necessary to take into account hundreds of quantum orbits. Note also that it is in this region that the threshold-related (channel closing) enhancements of HHG rates are most pronounced, for both s [13] and p states [43]. In contrast, HHG spectra for s and p states are very similar near and beyond the plateau cutoff. Concerning the variation of the rates with variation of the laser parameters, Fig. 4 allows us to formulate some general conclusions, valid for both s and p states.

(i) Plateau features in the HHG spectrum (as well as in the ATD spectrum) begin to develop for $\xi\equiv u_p/\omega>1$ [i.e., when PT in $V(\mathbf{r},t)$ breaks down [16,44]] and become well developed at $\xi\approx 5$. [Note that we have chosen the laser parameters in Fig. 4 such that $\xi=5.31$; 5.36; 5.38; and 1.90 for panels (a)–(d), respectively.]

(ii) The plateau cutoff position in HHG spectra is insensitive to the initial state symmetry (as is that for ATD [2]). This fact is consistent with the classical origin of the cutoff for all photon energies, including those comparable with the binding energy $|E_0|$, and is in agreement with our previous analysis for p states [16].

(iii) For fixed ξ [as, approximately, in panels (a)–(c)], the rates r_N decrease rapidly with decreasing ω (by a factor $\approx 10^{-5}$ as ω decreases from 0.20 to 0.10).

C. Symmetry effects in HHG spectra for fixed absolute laser parameters

As shown in the preceding section, for two ions (A and B) having a bound state of the same symmetry and for the same *scaled* F and ω, the ratio of HHG rates may be approximated with high accuracy as

$$\frac{\mathcal{R}_n^A}{\mathcal{R}_n^B}\approx\frac{\mathcal{C}_A}{\mathcal{C}_B}, \tag{35}$$

where the coefficients $\mathcal{C}$ (cf. Table II) are defined below Eq. (34). On the other hand, since the relation (35) involves different *absolute* values of laser frequency and intensity for each ion, it cannot be used to compare HHG rates for these ions for the same absolute laser parameters. In other words, although the curves in Fig. 4 describe the HHG rates for any ion with known E_0 and C_{kl} for the same *scaled* laser parameters, upon conversion to absolute units, the curves correspond to a different set of *absolute* laser parameters for each different ion. In order to compare the absolute HHG rates for different ions for the same set of absolute laser parameters, in Fig. 5 we present HHG spectra for eight negative ions for the low- [Figs. 5(a) and 5(b)] and high-frequency regimes [Figs. 5(c) and 5(d)]. Because of the significant difference in binding energies for ions with s and p outer electrons, the "low-frequency" results in Figs. 5(a) and 5(b) for ions with s electrons are given for $\lambda=10.6$ μm (the CO_2 laser), while the laser parameters for halogen ions are as in a recent experiment [39]: $\lambda=1.8$ μm and $I=10^{13}$ W/cm^2. Note that

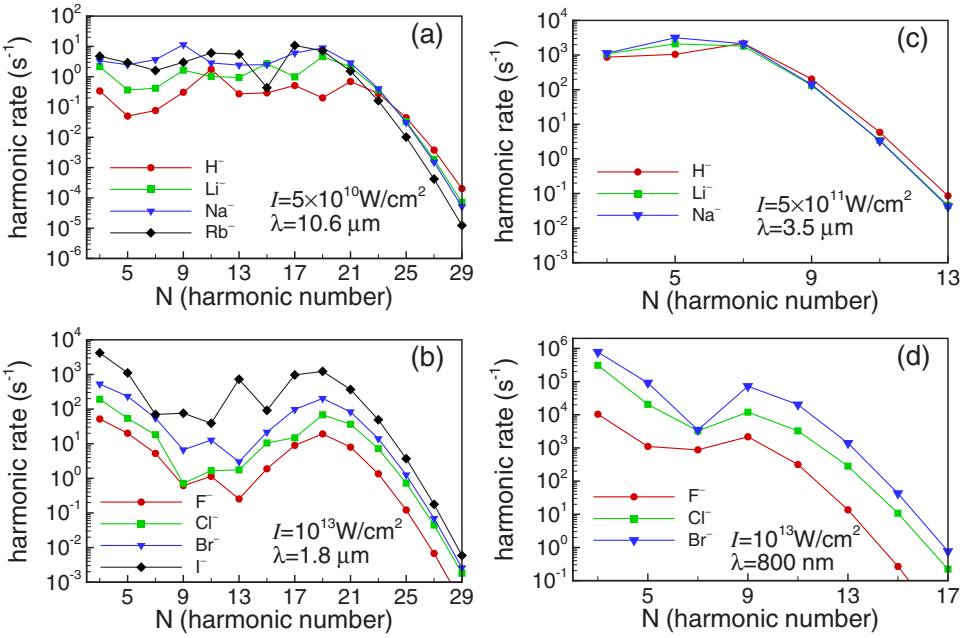

FIG. 5. (Color online) Absolute HHG rates for negative ions with s (a),(c) and p (b),(d) initial state symmetry for the wavelengths and intensities marked in the figures.

these low-frequency results are for approximately the same parameter $\xi=u_p/(\hbar\omega)$ in Figs. 5(a) (ξ=4.47) and 5(b) (ξ=4.37). To illustrate the dispersion of the *scaled* parameters for different ions at fixed *absolute* values of F and ω, we present these parameters in Table III for the data in Fig. 5.

For low frequencies [Figs. 5(a) and 5(b)], the rates for p electrons are (on average) much larger than those for s electrons, in agreement with the correspondingly large difference in the coefficients $\mathcal{C}$ in Table II for s and p states. In both cases one observes that the rates tend to increase as the atomic number of the ion increases, with the spread in the rates for p states being much greater than that for s states. This clear difference may stem from the greater dependence of HHG amplitudes on the initial state wave function (i.e., on the "inner dynamics") for p-state ions, as discussed above.

The existence of plateau structures in different laser-atom processes even for high frequencies has been shown recently in Ref. [16]. Figures 5(c) and 5(d) show such plateau structures in the HHG rates for both s- and p-state ions. As for the low-frequency case, the rates for s-state ions are much less than those for p-state ions; also, the spread in the rates for different ions is much greater for p-state ions. In contrast to the low-frequency case, however, the behavior of the rates $\mathcal{R}_N$ with increasing N is far smoother and less oscillatory. Such behavior is appropriate to the "multiphoton" regime (in contrast to the "tunneling" regime) of harmonic generation at high frequencies ($\hbar\omega<|E_0|$) [16]. Finally, we note that the plateau structures in the high-frequency HHG rates are "under-developed" [cf. Figs. 1(c), 1(d), 2(b), 4(d), 5(c), and 5(d)]. This stems, in part, from the small value of the parameter ξ for this regime ($\xi<2$). This parameter cannot be increased, however, for the frequencies considered, since with further increases in intensity, depletion of target ions over a laser cycle becomes significant [i.e., Γ exceeds $T^{-1}=\omega/(2\pi)$; this occurs already for Rb$^-$ and I$^-$ for the parameters used in Figs. 5(c) and 5(d)], and thus the concept of HHG rates loses its applicability.

V. SCALING OF HHG RATES FOR NEGATIVE IONS TO ATOMS

Although the results in Sec. III of paper I for the HHG amplitude in terms of complex quasienergy are valid for both

TABLE III. Scaled parameters ω and F for different ions at fixed absolute intensity (I) and wavelength (λ) of the laser field (cf. Fig. 5). $\tilde{I}=5\times10^{11}$ W/cm^2.

Ion (s state)	λ=10.6 μm $I=0.1\tilde{I}$	λ=3.5 μm $I=\tilde{I}$	Ion (p state)	λ=1.8 μm $I=20\tilde{I}$	λ=800 nm $I=20\tilde{I}$
H$^-$	ω=0.155	ω=0.470	F$^-$	ω=0.203	ω=0.456
	F=0.183	F=0.577		F=0.270	F=0.270
Li$^-$	ω=0.191	ω=0.579	Cl$^-$	ω=0.190	ω=0.428
	F=0.250	F=0.791		F=0.246	F=0.246
Na$^-$	ω=0.213	ω=0.644	Br$^-$	ω=0.204	ω=0.46
	F=0.294	F=0.928		F=0.273	F=0.273
Rb$^-$	ω=0.241	ω=0.729	I$^-$	ω=0.225	ω=0.505
	F=0.353	F=1.127		F=0.315	F=0.315

TABLE IV. Scaling factors $\mathcal{T}$ for scaling HHG rates for the F^- ion to Ne and Xe atoms subjected to a laser field with $I=2\times10^{14}$ W/cm^2 and $\lambda=800$ nm

Atom	ν	F/F_0	$\hbar\omega/\lvert E_a\rvert$	$\tilde{C}_{\kappa_a l}$	$\mathcal{T}$
Ne	0.794	0.076	0.072	1.300	3452
Xe	1.059	0.179	0.128	2.625	11600

atoms and ions, their application to atoms is a formidable task owing to the absence of analytical approximations for the complex quasienergy that account for the long-range Coulomb potential. Nevertheless, qualitative estimates of the role of Coulomb effects on the HHG process may be obtained similarly to those for tunneling ionization in Keldysh theory (cf. Refs. [45,46]). For strong field HHG, a Coulomb scaling factor was introduced in Ref. [37], but was not used to scale negative ion HHG rates to atoms. In this section we describe a scaling procedure that enables one to estimate HHG rates for an atomic electron having an energy $E_a=-\hbar^2\kappa_a^2/(2m)$ based on HHG rates for the outer electron of a negative ion with binding energy $E_0=-\hbar^2\kappa^2/(2m)$ and the same initial bound state symmetry as that for the active atomic electron. Existing results for Coulomb corrections to tunneling ionization rates are for the case of low frequencies (the quasistatic approximation), which we assume also. Moreover, it may be expected that atomic potential effects are most important for the low-energy part of the HHG spectrum, and that the HHG rates should be less sensitive to the atomic potential for harmonics near and beyond the classical cutoff.

As discussed in Sec. III (see also Ref. [15]), for the case of an *intense* low-frequency field, the HHG spectrum is well described by the KA, in which the dual dipole moment may be approximated by [cf. Eqs. (30) and (31) in paper I]

$$\tilde{\mathbf{d}}_{\mathrm{KA}}(t)\approx\langle\psi_0(\mathbf{r})|\mathbf{d}|\Phi_{\mathrm{KA}}(\mathbf{r},t)\rangle+\langle\tilde{\Phi}_{\mathrm{KA}}(\mathbf{r},t)|\mathbf{d}|\psi_0(\mathbf{r})\rangle, \tag{36}$$

where the KA wave function $\Phi_{\mathrm{KA}}(\mathbf{r},t)$ contains the entire dependence of the dual dipole moment on the laser intensity. As noted long ago [45,46] (see also Chap. V, Sec. IV in Ref. [21]), for the quasistatic (low-frequency) case, the modification of the wave function of a weakly bound electron in a laser field by long-range Coulomb forces reduces to only an intensity-dependent factor $\mathcal{T}_0$,

$$\mathcal{T}_0=(F_0/F)^{\nu}, \tag{37}$$

where $\nu=Z\sqrt{E_{\mathrm{H}}/\lvert E_a\rvert}$, $E_{\mathrm{H}}=13.606$ eV, Z is the charge of the remaining atomic core (i.e., $Z=0$ for negative ions and $Z=1$ for neutral atoms), and $F_0=\sqrt{2m\lvert E_a\rvert^3}/(\lvert e\rvert\hbar)$. Because the squares of the Fourier components of $\tilde{\mathbf{d}}_{\mathrm{KA}}(t)$ in Eq. (36) enter the HHG rate, the square of $\mathcal{T}_0$ enters the scaling factor $\mathcal{T}$ for scaling HHG rates for negative ions to atoms. (The Coulomb factor $\mathcal{T}_0^2$ was introduced also in Ref. [37] using arguments based on the three-step model for HHG.) In order to obtain the factor $\mathcal{T}$, differences in the asymptotic coefficients in the wave functions for negative ions and for atoms at $r\to\infty$ must be taken into account. They enter the HHG rate with the power four [37] [see also Eqs. (29)–(31)]. For negative ions, the definition of $C_{\kappa l}$ is given by Eq. (2); for an atom, the asymptotic coefficient $C_{\kappa_a l}$ is defined by $\varphi_{\kappa_a lm}(r\gg\kappa_a^{-1})\approx C_{\kappa_a l}r^{\nu-1}e^{-\kappa_a r}$. Thus the dimensionless coefficient $\mathcal{T}$ for atoms, which is used to scale the HHG rates (in s^{-1}) calculated for a negative ion at the same scaled frequency and laser field amplitude as for an atom, is given by

$$\mathcal{T}=(F_0/F)^{2\nu}(\tilde{C}_{\kappa_a l}/\tilde{C}_{\kappa l})^4(E_a/E_0)^2, \tag{38}$$

where the dimensionless asymptotic coefficients are $\tilde{C}_{\kappa_a l}=C_{\kappa_a l}/\kappa_a^{\nu+1/2}$ and $\tilde{C}_{\kappa l}=C_{\kappa l}/\sqrt{\kappa}$. Table IV gives the parameters necessary to calculate the parameter $\mathcal{T}$ that is needed to scale our exact TDER results for the F^- ion ($\lvert E_0\rvert=3.4$ eV, $\tilde{C}_{\kappa l}=1.188$) to the Ne ($\lvert E_a\rvert=21.56$ eV) and Xe ($\lvert E_a\rvert=12.13$ eV) atoms for the case of a laser field of intensity 2×10^{14} W/cm^2 and $\lambda=800$ nm [$u_p/(\hbar\omega)\approx7.7$]. Figure 6(a) compares our scaled results for Ne and Xe with those of Ref. [38], which are based on the use of realistic initial state wave functions. Our scaled results were obtained using the parameters in Table IV. Figure 6(a) shows that our scaled results are in good agreement with the results of Ref. [38] for harmonics at the high end of the plateau and beyond; moreover, as the scaled frequency becomes smaller (as for the case of Ne), our scaled results are in unexpectedly good agreement with the results of Ref. [38] over the entire plateau. The differences at small N may be attributed to inaccuracies of the quasiclassical analysis in Ref. [38] for low harmonics, $N<(1/\omega)$, as discussed in Sec. III.

Our analysis of the scaling factor must be modified for the case of a *not too strong* laser field ($u_p\approx\hbar\omega$), which corresponds to the onset of plateau structures in HHG spectra [15] (and for which the plateau region involves relatively few harmonics). For this case, the influence of the Coulomb field on the HHG rates should be much stronger than for the case of $u_p\gg\hbar\omega$. Moreover, the approximation (36) for the dual moment is not appropriate for this regime and a more accurate approximation,

$$\tilde{\mathbf{d}}(t)\approx\langle\tilde{\Phi}^{\mathrm{KA}}(\mathbf{r},t)|\mathbf{d}|\Phi^{\mathrm{KA}}(\mathbf{r},t)\rangle, \tag{39}$$

becomes necessary. [In fact, the approximation (39) takes into account the continuum-continuum transitions omitted in Eq. (36).] Thus an appropriate Coulomb scaling factor should be $\mathcal{T}_0^2$ times larger than $\mathcal{T}$,

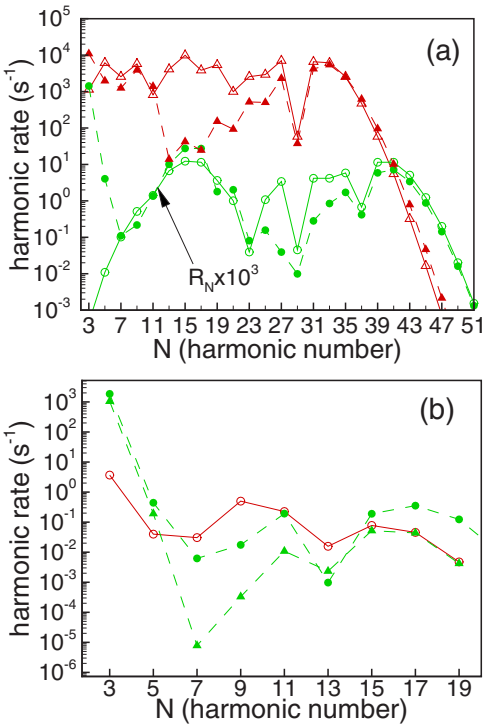

FIG. 6. (Color online) (a) HHG spectra for Ne and Xe for $I=2\times10^{14}$ W/cm^2 and $\lambda=800$ nm. Open symbols, results of Ref. [38] with realistic bound state wave functions; full symbols, our scaled results obtained from HHG rates for F^-. Circles, Ne; triangles, Xe. [Results of Ref. [38] are divided by 3 for consistency with Eq. (17).] (b) HHG spectra for the H atom ($1s$ state) for $\lambda=1064$ nm. Open circles, result of Ref. [47] for $I=1.4\times10^{13}$ W/cm^2; full circles and triangles, present results for H^- for $I=1.4\times10^{13}$ W/cm^2 and $I=1.1\times10^{13}$ W/cm^2, respectively, scaled by the factor $(16\pi/3)\mathcal{T}_1$ (see text for explanation).

$$\mathcal{T}_1=\mathcal{T}\mathcal{T}_0^2=(F_0/F)^{4\nu}(\tilde{C}_{\kappa_a l}/\tilde{C}_{\kappa l})^4(E_a/E_0)^2. \tag{40}$$

Figure 6(b) compares our scaled HHG rates for H^- ($|E_0|=0.755$ eV, $\tilde{C}_{\kappa l}=2.3$) with accurate numerical results of Ref. [47] for the H atom ($|E_a|=13.606$ eV, $\tilde{C}_{\kappa_a l}=2$) for a linearly polarized field of intensity $I=1.4\times10^{13}$ W/cm^2 and $\lambda=1064$ nm [$u_p/(\hbar\omega)=1.2$]. In order to get better cutoff matching, we also present scaled results for a lower intensity, $I=1.1\times10^{13}$ W/cm^2. Our scaled parameters are thus $F/F_0=0.040$, $\hbar\omega/|E_0|=0.086$, and $\mathcal{T}_1=1.9\times10^8$ for $I=1.4\times10^{13}$ W/cm^2, while $F/F_0=0.035$ and $\mathcal{T}_1=1.2\times10^8$ for $I=1.1\times10^{13}$ W/cm^2. [Owing to a difference of $16\pi/3$ between the definitions of HHG rates in Ref. [47] and in Eq. (17), our scaled results for the HHG rates in Fig. 6(b) were additionally multiplied by $16\pi/3$.] As expected for the weak-field regime, scaled rates for the low-order harmonics do not agree with those of Ref. [47], while plateau structures are sensitive to small variations of the intensity. However, for the plateau part of the HHG spectrum, scaled rates reproduce qualitatively the exact results in Ref. [47].

Our scaled numerical results show that, for the low-frequency regime ($\omega\leqslant0.1$), simple Coulomb factors (38) and (40) remove most of the differences between HHG rates for finite-range and Coulomb potentials. These differences range over several orders of magnitude, from about 10^4 for $u_p\gg\hbar\omega$ up to $\sim10^8$ for $u_p\approx\hbar\omega$. By means of these factors, HHG rates for atoms may thus be roughly estimated from accurate calculations for negative ions.

VI. SUMMARY AND CONCLUSIONS

The main results of this paper are (i) formal application of a wave-function-independent theoretical formulation of the HHG amplitude [1] to treat harmonic generation by a weakly bound electron in s and p states with exact account of strong field effects within the framework of TDER theory (cf. Sec. II); (ii) analysis and numerical use of the new TDER theory of HHG to make connections to commonly used approximate theories for HHG, to elucidate the dependence of HHG rates on initial state symmetry, and to compare and contrast HHG rates for a number of negative ions (cf. Secs. III and IV); and (iii) development of procedures to scale negative ion HHG rates to atoms (cf. Sec. V). In what follows we make some concluding remarks on this work.

In spite of the fact that the QQES wave function $\Phi_\epsilon(\mathbf{r},t)$ in TDER theory [2] is known only outside a short-range atomic core and thus cannot be used to calculate the dual dipole moment [which is defined by $\tilde{\mathbf{d}}(t)=\langle\tilde{\Phi}_\epsilon(t)|\hat{\mathbf{d}}|\Phi_\epsilon(t)\rangle$], the complex quasienergy may nevertheless be obtained as the eigenvalue of a one-dimensional integro-differential equation [cf. Eqs. (8) and (9)] for a periodic function $f_\epsilon(t)$ [which depends only on the boundary conditions satisfied by $\Phi_\epsilon(\mathbf{r},t)$]. As a result, we obtain an analytical expression (22) for the nonlinear susceptibility $\tilde{\chi}_N^{(m)}(\omega,F)$, which is the basic ingredient for our essentially analytical, self-consistent theory of HHG for a negative ion having an outer (weakly bound) electron of s or p symmetry. Only two parameters specify the concrete ion: the electron affinity, E_0, and the asymptotic coefficient $C_{\kappa l}$. For s-state ions it reduces to the ZRP model upon neglecting the effective range r_0. Although the exact HHG amplitude (22) is quite manageable for numerical computations, we have shown that its simplified version, the KA result (27), has high accuracy for the case of an intense low-frequency field and is thus convenient for large-scale calculations. This approximation neglects high-order binding potential effects and corresponds to the KA for QQES wave functions [15].

HHG rates for negative ions with s and p outer electrons show that the position of the plateau cutoff is insensitive to the initial state symmetry (even for high frequencies) and is given by the classical law, $\Omega_{\max}\approx|E_0|+3.17u_p$. However, the shape of the plateau strongly depends on this symmetry (e.g., oscillations of HHG rates along the plateau have opposite phases for p and s states). In fact, we find that the HHG rates are much more sensitive to the initial state symmetry than to the particular atomic species. (Note that for a given initial state symmetry, HHG rates are also much less sensitive to the atomic species than are rates for the competing above-threshold ionization process [15].) For the same scaled laser

parameters, HHG rates for p initial states are higher than for s states. This "enhancement" is mostly caused by differences in the asymptotic coefficients $C_{\kappa l}$ and binding energies for p-state and s-state ions, while the reduced rates r_N [cf. Eq. (34)], which are insensitive to these parameters, have on average approximately the same magnitude for negative halogen and alkali ions.

Since existing results for HHG rates for bound electrons with nonzero angular momentum have been obtained only with quasiclassical accuracy (in the framework of the three-step model [37,38]) and show a high sensitivity to the quality of initial bound state wave functions, we have performed a quasiclassical analysis of our exact results. For s states, our quasiclassical HHG amplitude exactly reproduces the three-step-model result in Ref. [33], whereas our results for p states are different from those in Ref. [37], where the asymptotic form (2) of the initial p-state wave function was used for the whole-space integration over the radial variable r. However, for low frequencies our quasiclassical results for p states are in reasonable agreement with results in Ref. [38], in which realistic initial state wave functions were employed.

Finally, we have described a simple scaling procedure that allows one to estimate atomic HHG rates by introducing Coulomb corrections to the results for negative ions. This scaling procedure is most appropriate for high-order harmonics produced by an intense low-frequency field. Also we have found that different scaling factors should be used for two different regimes of laser-atom interaction, $u_p \approx \hbar\omega$ and $u_p \gg \hbar\omega$.

ACKNOWLEDGMENTS

A number of valuable comments that have improved this paper as well as numerical data for Fig. 2 were provided to the authors by our colleague, V. N. Ostrovsky, who passed away recently. This work was supported in part by RFBR Grant No. 07-02-00574 and by NSF Grant No. PHY-0601196. Two of the authors (M.V.F. and A.V.F). acknowledge the support of the "Dynasty" Foundation, Grants of the President of the Russian Federation No. MK-1075.2005.2 and No. MK-8715.2006.2, and CRDF and BRHE Grants for young scientists, Grants No. Y2-P-10-03 and No. Y2-P-10-06. One of the authors (A.F.S.) gratefully acknowledges partial support of the Alexander von Humboldt Stiftung and the Max-Planck-Institut für Quantenoptik (MPQ) as well as the hospitality of the MPQ, where part of this paper was prepared.

APPENDIX A: EXPLICIT FORMS FOR $M^{(m)}_{k,k'}(\epsilon)$ AND $d^{(m)}_{\pm N;k,k'}$ IN EQS. (18) AND (19)

(1) The case of an s state $\psi_0(\mathbf{r})$ ($l=m=0$, $M^{(m)}_{k,k'} \equiv M_{k,k'}$, $d^{(m)}_{n;k,k'} \equiv d_{n;k,k'}$, $n \equiv \pm N$),

$$M_{k,k'}(\epsilon) = i^{k-k'}\sqrt{\frac{\omega}{8\pi i}}\int_0^\infty \frac{e^{2i(\epsilon/\omega+k+k')\phi}}{\phi^{3/2}}\{e^{-i\lambda(\phi)}J_{k-k'}[z(\phi)] - \delta_{k,k'}\}d\phi, \tag{A1}$$

$$d_{n;k,k'}(\epsilon) = \mathcal{C}_0\int_0^\infty \frac{d\phi}{\phi^{3/2}}e^{2i(\epsilon/\omega+k+k')\phi-i\lambda(\phi)}[j_-(\phi)\mathcal{J}_-(\phi) - ij_+(\phi)\mathcal{J}_+(\phi)], \tag{A2}$$

where $\mathcal{J}_\pm(\phi)$ is shorthand for the Bessel function, $\mathcal{J}_\pm(\phi) = J_{k-k'+(n\pm1)/2}[z(\phi)]$,

$$z(\phi) = \frac{2u_p}{\omega}\sin\phi\left(\cos\phi - \frac{\sin\phi}{\phi}\right),$$

$$\lambda(\phi) = \frac{2u_p}{\omega}\left(\phi - \frac{\sin^2\phi}{\phi}\right), \tag{A3}$$

$$j_\pm(\phi) = \frac{\sin\phi\sin(n\phi)}{\phi} - \frac{n\sin[(n\pm1)\phi]}{n\pm1}, \tag{A4}$$

$$\mathcal{C}_0 = \frac{2i^{k-k'+n/2}}{n^2}\sqrt{\frac{u_p}{\pi\omega^3}}, \quad u_p = \frac{F^2}{2\omega^2}. \tag{A5}$$

Note that $d_{n;k,k'}$ in Eq. (A2) formally coincides with the "susceptibility" $\tilde{\chi}_{n;k,k'}$ for a ZRP model presented in the Appendix of paper I: $d_{N;k,k'} = \tilde{\chi}_{n;k,k'}$. The difference is that the numerical value of the quasienergy ϵ in Eq. (A2) depends on the effective range r_0 [in accordance with Eq. (8)], while $r_0 = 0$ for a ZRP model.

(2) The case of a p state $\psi_0(\mathbf{r})$ ($l=1$; $m=0,\pm1$; $n \equiv \pm N$),

$$M^{(m)}_{k,k'}(\epsilon) = \bar{M}_{k,k'}(\epsilon) + \delta_{m,0}\hat{M}_{k,k'}(\epsilon), \tag{A6}$$

where

$$\bar{M}_{k,k'}(\epsilon) = \frac{3i^{k-k'+1}}{4}\sqrt{\frac{\omega^3}{8\pi i}}\int_0^\infty \frac{e^{2i(\epsilon/\omega+k+k')\phi}}{\phi^{5/2}}\{e^{-i\lambda(\phi)}J_{k-k'}[z(\phi)] - \delta_{k,k'}\}d\phi, \tag{A7}$$

$$\hat{M}_{k,k'}(\epsilon) = -3i^{k-k'}u_p\sqrt{\frac{\omega}{8\pi i}}\int_0^\infty \frac{e^{2i(\epsilon/\omega+k+k')\phi-i\lambda(\phi)}}{\phi^{3/2}}\{v_-(\phi)J_{k-k'}[z(\phi)] + iv_+(\phi)J'_{k-k'}[z(\phi)]\}d\phi. \tag{A8}$$

Matrix elements $d^{(m)}_{n;k,k'}$ have a general structure similar to that in Eq. (A6),

$$d^{(m)}_{n;k,k'} = \bar{d}_{n;k,k'}(\epsilon) + \delta_{m,0}\hat{d}_{n;k,k'}(\epsilon), \tag{A9}$$

where

$$\bar{d}_{n;k,k'}(\epsilon) = \frac{\mathcal{C}_1}{2n}\int_0^\infty d\phi \frac{e^{2i(\epsilon/\omega+k+k')\phi - i\lambda(\phi)}}{\phi^{5/2}}[j_-(\phi)\mathcal{J}_-(\phi) - ij_+(\phi)\mathcal{J}_+(\phi)], \tag{A10}$$

$$\hat{d}_{n;k,k'}(\epsilon) = \mathcal{C}_1\int_0^\infty d\phi \frac{e^{2i(\epsilon/\omega+k+k')\phi - i\lambda(\phi)}}{\phi^{3/2}}\Big(v_{-,n}(\phi)\mathcal{J}_-(\phi) - iv_{+,n}(\phi)\mathcal{J}_+(\phi) + \frac{2u_p}{n\omega}\{ij_-(\phi)[v_-(\phi)\mathcal{J}_-(\phi) + iv_+(\phi)\mathcal{J}'_-(\phi)] + j_+(\phi)[v_-(\phi)\mathcal{J}_+(\phi) + iv_+(\phi)\mathcal{J}'_+(\phi)]\}\Big), \tag{A11}$$

and where $\mathcal{J}'_\pm(\phi)$ is the derivative of $\mathcal{J}_\pm(\phi)$ over the argument $z(\phi)$,

$$v_{\pm,n}(\phi) = \left(\frac{\sin(n\phi)}{n\phi} - \cos(n\phi)\right)\left(\frac{\sin\phi}{\phi} - \cos\phi\right) \pm \sin(n\phi)\sin\phi, \tag{A12}$$

$$v_\pm(\phi) \equiv v_{\pm,n=1}(\phi) = \left(\frac{\sin\phi}{\phi} - \cos\phi\right)^2 \pm \sin^2\phi, \quad \mathcal{C}_1 = \frac{3i^{k-k'+1+n/2}}{n}\sqrt{\frac{u_p}{\pi\omega}}. \tag{A13}$$

APPENDIX B: QUASICLASSICAL HHG AMPLITUDE IN TDER THEORY

In order to carry out the quasiclassical analysis of the HHG amplitude sketched in Sec. III B, we represent the integral term on the right-hand side of Eq. (4) in terms of the quasienergy representation for the Green function, $\mathcal{G}^{(V)}_\epsilon(\mathbf{r},t;\mathbf{r}',t')$, of a free electron in the field $\tilde{\mathbf{F}}(t)$ given by Eq. (7). Its spectral expansion has a known form [48,49] [absolute units are used in Eqs. (B1)–(B3)],

$$\mathcal{G}^{(V)}_\epsilon(\mathbf{r},t;\mathbf{r}',t') = \sum_{s=-\infty}^{\infty}\int d\mathbf{p}\frac{\chi_{\mathbf{p},s}(\mathbf{r},t)\chi^*_{\mathbf{p},s}(\mathbf{r}',t')}{\epsilon - E_{p,s} + i0}, \tag{B1}$$

where $E_{p,s}=E_p+s\hbar\omega+\tilde{u}_p$; $E_p=\mathbf{p}^2/(2m)$; $\tilde{u}_p=(e^2F^2)/(4m\omega^2)+(e^2F_h^2)/(4m\Omega^2)$; and $\chi_{\mathbf{p},s}(\mathbf{r},t)=\chi_{\mathbf{p}}(\mathbf{r},t)\exp(is\omega t)$. The function $\chi_{\mathbf{p},s}(\mathbf{r},t)$ is the solution of Eq. (1) with $U(\mathbf{r})=0$ and $V(\mathbf{r},t)=-\mathbf{d}\cdot\tilde{\mathbf{F}}(t)$, which relates to the common Volkov wave function $\Psi^{(V)}_{\mathbf{p}}(\mathbf{r},t)$ [normalized by $1/\sqrt{(2\pi\hbar)^3}$] as follows: $\Psi^{(V)}_{\mathbf{p}}(\mathbf{r},t)=\chi_{\mathbf{p},s}(\mathbf{r},t)\exp[-(i/\hbar)E_{p,s}t]$. The desired relation,

$$\int_{-\infty}^{t} G^{(V)}(\mathbf{r},t;\mathbf{r}',t')f(t')e^{i\epsilon(t-t')/\hbar}dt' = \frac{1}{T}\int_0^T \mathcal{G}^{(V)}_\epsilon(\mathbf{r},t;\mathbf{r}',t')f(t')dt', \tag{B2}$$

follows immediately from the known relation between $\mathcal{G}^{(V)}_\epsilon$ and the usual time-dependent (Volkov) Green function, $G^{(V)}$ [48,49],

$$\mathcal{G}^{(V)}_\epsilon(\mathbf{r},t;\mathbf{r}',t') = T\sum_{k=-\infty}^{\infty} G^{(V)}(\mathbf{r},t;\mathbf{r}',t'-kT)\times\exp\left(\frac{i}{\hbar}\epsilon(t-t'+kT)\right), \tag{B3}$$

upon multiplying Eq. (B3) by the periodic function $f(t')$ and integrating over t' over the period $T=2\pi/\omega$. (The relation (B2) is a common one for representing the basic integral equations of QQES theory in terms of either $\mathcal{G}^{(V)}_\epsilon$ or $G^{(V)}$ [48,49]; it may also be obtained using the so-called "factorization techniques" [50] (used for HHG calculations in Ref. [33]) which, indeed, amounts "to some special representation of [the] time-dependent Green function" [i.e., given by Eq. (B3)], as suspected by the authors of Ref. [33].)

The integral over $\mathbf{p}$ in Eq. (B1) may be calculated analytically in closed form, so that the right-hand side of Eq. (B2) may be written as follows [details of the calculation are similar to those in Ref. [33] for the case of a single-frequency field, $\mathbf{F}(t)$]:

$$\chi^{\mathrm{KA}}(\mathbf{r},\mathbf{r}';t) \equiv \frac{1}{T}\int_0^T \mathcal{G}^{(V)}_\epsilon(\mathbf{r},t;\mathbf{r}',t')dt' = -\frac{1}{4\pi}\sum_s\frac{1}{T}\int_0^T dt'\frac{e^{i\tilde{\mathcal{S}}_s(\mathbf{r},t;\mathbf{r}',t')}}{|\mathbf{R}-\mathbf{R}'|}, \tag{B4}$$

where

$$\tilde{\mathcal{S}}_s(\mathbf{r},t;\mathbf{r}',t') = \mathbf{r}\cdot\dot{\boldsymbol{\mathcal{R}}}(t) - \mathbf{r}'\cdot\dot{\boldsymbol{\mathcal{R}}}(t') + k_s|\mathbf{R}-\mathbf{R}'| - \int_{t'}^{t}[\dot{\boldsymbol{\mathcal{R}}}(\tau)^2 - \tilde{u}_p + s\omega]d\tau,$$

$$k_s = \sqrt{\tilde{\epsilon}+s\omega-\tilde{u}_p}, \quad \mathbf{R}=\mathbf{r}-2\boldsymbol{\mathcal{R}}(t), \quad \mathbf{R}'=\mathbf{r}'-2\boldsymbol{\mathcal{R}}(t'),$$

$$\boldsymbol{\mathcal{R}}(t) = \mathbf{e}_z\mathcal{R}(t), \quad \mathcal{R}(t) = \frac{F\cos(\omega t)}{\omega^2} + \frac{F_h\cos(\Omega t)}{\Omega^2}, \quad \Omega = N\omega. \tag{B5}$$

The KA-like wave function $\Phi^{\mathrm{KA}}_{\tilde{\epsilon}}(\mathbf{r},t)$ is obtained from $\chi^{\mathrm{KA}}(\mathbf{r},\mathbf{r}';t)$ according to Eq. (4) [upon substituting $f_\epsilon(t')\to 1$]. Its explicit forms for s and p initial states, $\psi_0(\mathbf{r})$, are

$$\Phi^{(s)}(\mathbf{r},t) = \frac{1}{\sqrt{4\pi}}\sum_s\frac{1}{T}\int_0^T dt' e^{i\tilde{\mathcal{S}}_s(\mathbf{r},t;0,t')}\frac{1}{|\tilde{\mathbf{R}}(t,t')|}, \tag{B6}$$

$$\Phi_m^{(p)}(\mathbf{r},t)=\sum_s \frac{1}{T}\int_0^T dt' e^{i\tilde{\mathcal{S}}_s(\mathbf{r},t;0,t')}\Bigg[rY_{1m}(\hat{r})\frac{1-ik_s|\tilde{\mathbf{R}}(t,t')|}{|\tilde{\mathbf{R}}(t,t')|^3} - \delta_{m,0}\sqrt{\frac{3}{4\pi}}\Bigg(i\frac{\dot{\mathcal{R}}(t')}{|\tilde{\mathbf{R}}(t,t')|}+2\frac{1-ik_s|\tilde{\mathbf{R}}(t,t')|}{|\tilde{\mathbf{R}}(t,t')|^3}[\mathcal{R}(t) - \mathcal{R}(t')]\Bigg)\Bigg], \quad m=0,\pm 1, \tag{B7}$$

where $\tilde{\mathbf{R}}(t,t')=\mathbf{R}+2\boldsymbol{\mathcal{R}}(t')=\mathbf{r}-2\mathbf{e}_z[\mathcal{R}(t)-\mathcal{R}(t')]$. Since the harmonic field $\mathbf{F}_h(t)$ is weak $(F_h\to 0)$, we approximate $\tilde{u}_p$ by $u_p=F^2/(2\omega^2)$, so that $k_s=\sqrt{\tilde{\epsilon}+s\omega-u_p}$ and the dependence of $\Phi^{(s)}$ and $\Phi_m^{(p)}$ on F_h is contained only in the factors $\mathcal{R}(t)$, $\mathcal{R}(t')$ [including those in $\tilde{\mathcal{S}}_s(\mathbf{r},t;0,t')$].

According to the boundary condition (5), the QQES wave function in TDER theory diverges at small distances, so that the functions (B6) and (B7) are singular at $r=0$. To extract the singular terms explicitly, we use the following identities:

$$\frac{1}{T}\sum_s\int_0^T \frac{e^{i\varphi(t')-i\varphi(t)-is\omega(t-t')}}{|\tilde{\mathbf{R}}(t,t')|^\nu}dt'=\frac{1}{r^\nu},$$

$$\varphi(t)=\int^t[\dot{\mathcal{R}}^2(\tau)-u_p]d\tau,$$

$$\frac{1}{T}\sum_s\int_0^T \frac{se^{i\varphi(t')-i\varphi(t)-is\omega(t-t')}}{|\tilde{\boldsymbol{\mathcal{R}}}(t,t')|^\nu}dt'=\frac{i}{\omega}\left(\frac{i\dot{\varphi}(t)}{r^\nu}-\frac{2\nu\mathbf{r}\cdot\dot{\boldsymbol{\mathcal{R}}}(t)}{r^{\nu+2}}\right), \tag{B8}$$

where we have used a known relation for the δ-function in a space of periodic functions,

$$\delta(t-t')=(1/T)\sum_s e^{-is\omega(t-t')}. \tag{B9}$$

Using Eq. (B8), the functions (B6) and (B7) can be represented in the following form:

$$\Phi^{(s)}(\mathbf{r},t)=\frac{1}{\sqrt{4\pi}}\exp[i\mathbf{r}\cdot\dot{\boldsymbol{\mathcal{R}}}(t)]\left(\frac{1}{r}+\sum_s\frac{1}{T}\int_0^T e^{-i\int_{t'}^t[\dot{\mathcal{R}}^2(\tau)-u_p+s\omega]d\tau}\frac{\{\exp[ik_s|\tilde{\mathbf{R}}(t,t')|]-1\}}{|\tilde{\mathbf{R}}(t,t')|}dt'\right), \tag{B10}$$

$$\Phi_m^{(p)}(\mathbf{r},t)=Y_{1m}(\hat{r})\exp[i\mathbf{r}\cdot\dot{\boldsymbol{\mathcal{R}}}(t)]\left(\frac{1-i\mathbf{r}\cdot\dot{\boldsymbol{\mathcal{R}}}(t)}{r^2}-\frac{\dot{\mathcal{R}}^2(t)}{2}+\frac{\tilde{\epsilon}}{2}\right)+rY_{1m}(\hat{r})\exp[i\mathbf{r}\cdot\dot{\boldsymbol{\mathcal{R}}}(t)]$$
$$\times\sum_s\frac{1}{T}\int_0^T e^{-i\int_{t'}^t[\dot{\mathcal{R}}^2(\tau)-u_p+s\omega]d\tau}\frac{1}{|\tilde{\mathbf{R}}(t,t')|^3}\left(\exp[ik_s|\tilde{\mathbf{R}}(t,t')|][1-ik_s|\tilde{\mathbf{R}}(t,t')|]-\frac{1}{2}k_s^2\tilde{\mathbf{R}}^2(t,t')-1\right)dt'$$
$$-\delta_{m,0}i\sqrt{\frac{3}{4\pi}}\exp[i\mathbf{r}\cdot\dot{\boldsymbol{\mathcal{R}}}(t)]\sum_s\frac{1}{T}\int_0^T e^{-i\int_{t'}^t[\dot{\mathcal{R}}^2(\tau)-u_p+s\omega]d\tau}\left(\frac{\{\exp[ik_s|\tilde{\mathbf{R}}(t,t')|]-1\}\dot{\mathcal{R}}(t')}{|\tilde{\mathbf{R}}(t,t')|}\right.$$
$$\left.+[\mathcal{R}(t)-\mathcal{R}(t')]\frac{2\exp[ik_s|\tilde{\mathbf{R}}(t,t')|][1-ik_s|\tilde{\mathbf{R}}(t,t')|]-k_s^2\tilde{\mathbf{R}}^2(t,t')-2}{|\tilde{\mathbf{R}}(t,t')|^3}\right)dt'. \tag{B11}$$

The integral terms in Eqs. (B10) and (B11) are regular at the origin ($r=0$), and thus the integration path over t' can be shifted into the complex t' plane in order to integrate over t' by the stationary phase method at any r. We deform this path so that it passes through the stationary phase points, t'_ν, of the function $\tilde{\mathcal{S}}_s(\mathbf{r}=0,t;\mathbf{r}'=0,t')\equiv\tilde{\mathcal{S}}_s(t;t')$ in Eq. (B5). This function may be represented as follows:

$$\tilde{\mathcal{S}}_s(t;t')\equiv 2k_s|\boldsymbol{\mathcal{R}}(t)-\boldsymbol{\mathcal{R}}(t')|-\int_{t'}^t[\dot{\boldsymbol{\mathcal{R}}}(\tau)^2-\tilde{u}_p+s\omega]d\tau$$
$$=\tilde{\mathcal{S}}_s(t')-\tilde{\mathcal{S}}_s(t), \tag{B12}$$

where

$$\tilde{\mathcal{S}}_s(t')=\int^{t'}\{[\tilde{\mathbf{K}}_s-\dot{\boldsymbol{\mathcal{R}}}(\tau)]^2-\tilde{\epsilon}\}d\tau,$$

$$\tilde{\mathbf{K}}_s=k_s\frac{\boldsymbol{\mathcal{R}}(\tau)-\boldsymbol{\mathcal{R}}(t')}{|\boldsymbol{\mathcal{R}}(\tau)-\boldsymbol{\mathcal{R}}(t')|}=k_s\hat{n}, \tag{B13}$$

and where $\hat{n}$ is the unit vector directed along the vector $[\boldsymbol{\mathcal{R}}(\tau)-\boldsymbol{\mathcal{R}}(t')]$, i.e., $\hat{n}=\pm\mathbf{e}_z$. Thus the equation for t'_ν is

$$\tilde{\mathcal{S}}'_s(t'_\nu)=[\tilde{\mathbf{K}}_s-\dot{\boldsymbol{\mathcal{R}}}(t'_\nu)]^2-\tilde{\epsilon}=0, \quad \tilde{\mathbf{K}}_s=\pm k_s\mathbf{e}_z. \tag{B14}$$

Since $\mathrm{Re}\,\tilde{\epsilon}<0$, the equation (B14) has only complex solutions, t'_ν. Moreover, for each of the two directions of the vector $\tilde{\mathbf{K}}_s$, there are two solutions, t'_ν, symmetric with respect to the real axis of t'. Furthermore, only the solutions with

positive imaginary parts, $\mathrm{Im}\, t'_\nu > 0$, should be taken into account (see Sec. III in Ref. [33] for details). Thus, for each direction of $\tilde{\mathbf{K}}_s$, only one saddle point t'_ν contributes to the integrals over t' in Eqs. (B10) and (B11) by the stationary phase method.

Besides the general quasiclassical condition, $\omega \ll 1$, the quasiclassical analysis of HHG requires also the condition [33], $F/\omega^2 \gg 1$ [or, in absolute units, $\alpha_0 \gg \kappa^{-1}$, where $\alpha_0 = (eF)/(m\omega^2)$ is the amplitude of free electron oscillations in a laser field]. Therefore, the factor $[\mathcal{R}(t) - \mathcal{R}(t'_\nu)]$ must be treated as a large (complex) parameter in our further considerations. For small r, $r \approx r_c \ll 1$, we expand the integral terms on the right-hand sides of Eqs. (B10) and (B11) in the small parameter $r|\mathcal{R}(t) - \mathcal{R}(t'_\nu)|^{-1}$ up to terms of order r^l [cf. Eq. (5)], project the results on the spherical harmonic $Y_{lm}(\hat{r})$, and average the resulting expressions for functions (B10) and (B11) over time t over the period T. Then, performing the integration over t' using the stationary phase method and matching the results with the boundary condition (5) at $f_n = \delta_{n,0}$, we obtain the following results for $\Delta\epsilon = \tilde{\epsilon} - E_0$: For the s state $\psi_0(\mathbf{r})$,

$$\Delta\epsilon = -\frac{C_{\kappa 0}^2}{T^2} \sum_{s,\nu} \sqrt{\frac{\pi i}{2\tilde{S}''_s(t'_\nu)}}\, e^{i\tilde{S}_s(t'_\nu)} \int_0^T \frac{e^{-i\tilde{S}_s(t)}}{|\mathcal{R}(t) - \mathcal{R}(t'_\nu)|}\, dt, \tag{B15}$$

and for the p state $\psi_0(\mathbf{r})$,

$$\Delta\epsilon = \frac{3C_{\kappa 1}^2}{T^2} \sum_{s,\nu} \sqrt{\frac{\pi i}{2\tilde{S}''_s(t'_\nu)}}\, e^{i\tilde{S}_s(t'_\nu)} \int_0^T e^{-i\tilde{S}_s(t)} \left(\delta_{|m|,1} \frac{ik_s}{|\mathcal{R}(t) - \mathcal{R}(t'_\nu)|^2} - \delta_{m,0} \frac{[\dot{\mathcal{R}}(t'_\nu) - \mathbf{K}_s] \cdot [\dot{\mathcal{R}}(t) - \mathbf{K}_s]}{|\mathcal{R}(t) - \mathcal{R}(t'_\nu)|} \right) dt. \tag{B16}$$

In Eqs. (B15) and (B16) we have approximated $(-1)^{l+1}[1 - (-\epsilon)^{(2l+1)/2}] + r_l \Delta\epsilon/2 \approx -\Delta\epsilon/C_{\kappa l}^2$ and replaced ϵ by E_0 in k_s, i.e., $k_s = \sqrt{s\omega - 1 - u_p}$. Also, only terms of lowest order in $|\mathcal{R}(t) - \mathcal{R}(t'_\nu)|^{-1}$ were kept on the right-hand sides of Eqs. (B15) and (B16). To extract the linear in F_h terms in $\Delta\epsilon$, we integrate by parts in Eqs. (B15) and (B16) using the following approximate [i.e., lowest order in $|\mathcal{R}(t) - \mathcal{R}(t'_\nu)|^{-1}$] relations:

$$\int_0^T \frac{e^{-i\tilde{S}_s(t)} g_p[\dot{\mathcal{R}}(t)]}{|\mathcal{R}(t) - \mathcal{R}(t'_\nu)|^{1+|m|}}\, dt \approx i\omega^2 \int_0^T \frac{e^{-iS_s(t)}[F(t) + F_h(t)]}{|\mathbf{F}(t) - \mathbf{F}(t'_\nu)|^{1+|m|}} \frac{\partial}{\partial k_t} \left(\frac{g_p(k_t)}{S'_s(t)} \right) dt, \tag{B17}$$

where

$$F(t) + F_h(t) = -\ddot{\mathcal{R}}(t), \quad g_0[\dot{\mathcal{R}}(t)] = g_0(k_t) = 1, \quad g_1[\dot{\mathcal{R}}(t)] = \dot{\mathcal{R}}(t) \pm k_s, \quad g_1(k_t) = k_t \pm k_s, \quad \mathbf{k}_t = \dot{\mathbf{F}}(t)/\omega^2 = -\mathbf{e}_z F/\omega \sin \omega t.$$

Since the right-hand side of Eq. (B17) explicitly involves $F_h(t)$ in the numerator, the substitution $\mathcal{R}(t) \to \mathbf{F}(t)/\omega^2$ had been made in all other places on the right-hand side of Eq. (B17), including $\tilde{S}_s(t) \to S_s(t)$, where [cf. Eq. (B13)]

$$S_s(t) = \int^t [(\mathbf{K}_s - \mathbf{k}_\tau)^2 + 1]\, d\tau, \quad \mathbf{K}_s = k_s \frac{\mathbf{F}(t) - \mathbf{F}(t')}{|\mathbf{F}(t) - \mathbf{F}(t')|} = \pm k_s \mathbf{e}_z. \tag{B18}$$

Correspondingly, $\tilde{S}_s(t'_\nu)$ in Eqs. (B15) and (B16) should also be replaced by $S_s(t'_\nu)$. Thus instead of (B14), the stationary phase points t'_ν in Eqs. (B15) and (B16) should be determined from the equation $S'_s(t'_\nu) = 0$, which involves only the laser field $\mathbf{F}(t)$.

Extracting the linear in F_h terms in $\Delta\epsilon$ in Eqs. (B15) and (B16) using Eq. (B17), the HHG amplitude is obtained from relations similar to Eqs. (15) and (16). After some algebra, we obtain the following results: For an s state $\psi_0(\mathbf{r})$,

$$A_N^{(s)} = 2i \sum_{s,\nu} Z_{0,s} \int_0^T \frac{e^{i[\Omega t + S_s(t'_\nu) - S_s(t)]} (\mathbf{k}_t - \mathbf{K}_s) \cdot \mathbf{e}'^*}{|\cos(\omega t) - \cos(\omega t'_\nu)| [(\mathbf{K}_s - \mathbf{k}_t)^2 + 1]^2}\, dt, \tag{B19}$$

and for a p state $\psi_0(\mathbf{r})$,

$$A_N^{(p,|m|=1)} = \frac{\omega^2}{F} \sum_{s,\nu} Z_{1,s} k_s \int_0^T \frac{e^{i[\Omega t + S_s(t'_\nu) - S_s(t)]} (\mathbf{k}_t - \mathbf{K}_s) \cdot \mathbf{e}'^*}{|\cos(\omega t) - \cos(\omega t'_\nu)|^2 [(\mathbf{K}_s - \mathbf{k}_t)^2 + 1]^2}\, dt, \tag{B20}$$

$$A_N^{(p,m=0)} = \sum_{s,\nu} Z_{1,s} \int_0^T \frac{e^{i[\Omega t + S_s(t'_\nu) - S_s(t)]} [(\mathbf{K}_s - \mathbf{k}_t)^2 - 1] (\mathbf{K}_s - \mathbf{k}_{t'_\nu}) \cdot \mathbf{e}'^*}{|\cos(\omega t) - \cos(\omega t'_\nu)| [(\mathbf{K}_s - \mathbf{k}_t)^2 + 1]^2}\, dt, \tag{B21}$$

where

$$Z_{l,s} = \frac{(2l+1)C_{\kappa l}^2 \omega^4}{4\pi^2 F} \sqrt{\frac{2\pi i}{S''_s(t'_\nu)}}.$$

Note that the generalization to the case of an arbitrary polarization of the harmonic field, $\mathbf{e}'$, in Eqs. (B19)–(B21) was done by substituting $\mathbf{e}_z \to \mathbf{e}'^*$, as explained below Eqs. (28) and (29) in paper I. The sum Σ_s is taken over all open s-photon ATI channels, i.e., those with $s > (u_p+1)/\omega$. As argued in Ref. [33], the sum Σ_ν over two stationary points, t'_ν [corresponding to the two opposite directions of $\mathbf{K}_s$ in (B18)], may be replaced by the contribution of only one of these points (e.g., that with the smaller value of $\mathrm{Re}\, t'_\nu > 0$, say t'_0), multiplying the expressions (B19)–(B21) by a factor of 2 and substituting $|\cos(\omega t) - \cos(\omega t'_\nu)| \to [\cos(\omega t) - \cos(\omega t'_0)]$ in the denominators. As a result, the final quasiclassical expressions for the HHG amplitudes attain the forms (29)–(31) given in the main text.

[1] M. V. Frolov, A. V. Flegel, N. L. Manakov, and A. F. Starace, Phys. Rev. A **75**, 063407 (2007), preceding paper.
[2] M. V. Frolov, N. L. Manakov, E. A. Pronin, and A. F. Starace, Phys. Rev. Lett. **91**, 053003 (2003).
[3] M. V. Frolov, N. L. Manakov, E. A. Pronin, and A. F. Starace, J. Phys. B **36**, L419 (2003).
[4] W. Becker, F. Grabson, R. Kopold, D. B. Milošević, G. G. Paulus, and H. Walther, Adv. At., Mol., Opt. Phys. **48**, 35 (2002).
[5] N. L. Manakov and A. G. Fainshtein, Zh. Eksp. Teor. Fiz. **79**, 751 (1980) [Sov. Phys. JETP **52**, 382 (1980)].
[6] N. L. Manakov, M. V. Frolov, A. F. Starace, and I. I. Fabrikant, J. Phys. B **33**, R141 (2000).
[7] N. L. Manakov, M. V. Frolov, B. Borca, and A. F. Starace, J. Phys. B **36**, R49 (2003).
[8] W. Becker, S. Long, and J. K. McIver, Phys. Rev. A **41**, 4112 (1990).
[9] W. Becker, S. Long, and J. K. McIver, Phys. Rev. A **46**, R5334 (1992).
[10] W. Becker, S. Long, and J. K. McIver, Phys. Rev. A **50**, 1540 (1994).
[11] B. Borca, A. V. Flegel, M. V. Frolov, N. L. Manakov, D. B. Milošević, and A. F. Starace, Phys. Rev. Lett. **85**, 732 (2000).
[12] B. Borca, D. B. Milošević, A. F. Starace, A. V. Flegel, M. V. Frolov, and N. L. Manakov, in *Super-Intense Laser-Atom Physics*, edited by B. Piraux and K. Rzażewsky, NATO Sci. Ser. II: Math., Phys. and Chemistry, Vol. 12 (Kluwer, Dordrecht, 2001), p. 249.
[13] B. Borca, A. F. Starace, A. V. Flegel, M. V. Frolov, and N. L. Manakov, Phys. Rev. A **65**, 051402(R) (2002).
[14] A. V. Flegel, M. V. Frolov, N. L. Manakov, and A. F. Starace, J. Phys. B **38**, L27 (2005).
[15] M. V. Frolov, A. A. Khuskivadze, N. L. Manakov, and A. F. Starace, J. Phys. B **39**, S283 (2006).
[16] M. V. Frolov, A. V. Flegel, N. L. Manakov, and A. F. Starace, J. Phys. B **38**, L375 (2005).
[17] S. Beiser, M. Klaiber, and I. Y. Kiyan, Phys. Rev. A **70**, 011402(R) (2004).
[18] D. Bauer, D. B. Milošević, and W. Becker, Phys. Rev. A **72**, 023415 (2005).
[19] K. Krajewska, I. I. Fabrikant, and A. F. Starace, Phys. Rev. A **74**, 053407 (2006).
[20] Yu. N. Demkov and V. N. Ostrovsky, *Zero-Range Potentials and Their Applications in Atomic Physics* (Plenum, New York, 1988).
[21] A. I. Baz', Ya. B. Zel'dovich, and A. M. Perelomov, *Scattering, Reactions and Decays in Nonrelativistic Quantum Mechanics*, 2nd ed. (Nauka, Moscow, 1971) (in Russian).
[22] S. P. Andreev, B. M. Karnakov, V. D. Mur, and V. A. Polunin, Zh. Eksp. Teor. Fiz. **86**, 866 (1984) [Sov. Phys. JETP **59**, 506 (1984)].
[23] Yu. N. Demkov and G. F. Drukarev, Zh. Eksp. Teor. Fiz. **81**, 1218 (1981) [Sov. Phys. JETP **54**, 650 (1981)].
[24] L. D. Landau and E. M. Lifshitz, *Quantum Mechanics*, 4th ed. (Pergamon, Oxford, 1992).
[25] M. L. Du and J. B. Delos, Phys. Rev. A **38**, 5609 (1988).
[26] A. A. Radzig and B. M. Smirnov, *Reference Data on Atoms, Molecules and Ions* (Springer, Berlin, 1985).
[27] L. V. Keldysh, Zh. Eksp. Teor. Fiz. **47**, 1945 (1964) [Sov. Phys. JETP **20**, 1307 (1965)].
[28] V. S. Popov, Usp. Fiz. Nauk **174**, 921 (2004) [Phys. Usp. **47**, 855 (2004)].
[29] A. I. Nikishov and V. I. Ritus, Zh. Eksp. Teor. Fiz. **50**, 255 (1966) [Sov. Phys. JETP **23**, 168 (1966)].
[30] A. M. Perelomov, V. S. Popov, and M. V. Terent'ev, Zh. Eksp. Teor. Fiz. **50**, 1393 (1966) [Sov. Phys. JETP **23**, 924 (1966)].
[31] G. F. Gribakin and M. Yu. Kuchiev, Phys. Rev. A **55**, 3760 (1997).
[32] W. Becker, A. Lohr, M. Kleber, and M. Lewenstein, Phys. Rev. A **56**, 645 (1997).
[33] M. Yu. Kuchiev and V. N. Ostrovsky, Phys. Rev. A **60**, 3111 (1999).
[34] M. Lewenstein, P. Balcou, M. Yu. Ivanov, A. L'Huillier, and P. B. Corkum, Phys. Rev. A **49**, 2117 (1994).
[35] M. Yu. Kuchiev and V. N. Ostrovsky, J. Phys. B **32**, L189 (1999).
[36] M. Yu. Kuchiev and V. N. Ostrovsky, J. Phys. B **34**, 405 (2001).
[37] V. N. Ostrovsky and J. B. Greenwood, J. Phys. B **38**, 1867 (2005).
[38] V. N. Ostrovsky, J. Phys. B **38**, 4399 (2005).
[39] R. Reichle, H. Helm, and I. Yu. Kiyan, Phys. Rev. Lett. **87**, 243001 (2001).
[40] J. Pedregosa-Gutierrez, P. A. Orr, J. B. Greenwood, A. Murphy, J. T. Costello, K. Zrost, T. Ergler, R. Moshammer, and J. Ullrich, Phys. Rev. Lett. **93**, 223001 (2004).
[41] V. N. Ostrovsky (private communication).
[42] D. B. Milošević and W. Becker, Phys. Rev. A **66**, 063417 (2002).
[43] N. L. Manakov and M. V. Frolov, Pis'ma Zh. Eksp. Teor. Fiz.

83, 630 (2006) [JETP Lett. **83**, 536 (2006)].
[44] N. L. Manakov and A. G. Fainshtein, Dokl. Akad. Nauk SSSR **244**, 567 (1979) [Sov. Phys. Dokl. **24**, 41 (1979)].
[45] A. M. Perelomov and V. S. Popov, Zh. Eksp. Teor. Fiz. **52**, 514 (1967) [Sov. Phys. JETP **25**, 336 (1967)].
[46] V. S. Popov, V. P. Kuznetsov, and A. M. Perelomov, Zh. Eksp. Teor. Fiz. **53**, 331 (1967) [Sov. Phys. JETP **26**, 222 (1968)].
[47] E. Mese and R. M. Potvliege, J. Phys. B **39**, 431 (2006).
[48] N. L. Manakov, V. D. Ovsiannikov, and L. P. Rapoport, Phys. Rep. **141**, 319 (1986).
[49] N. L. Manakov and A. G. Fainshtein, Teor. Mat. Fiz. **48**, 375 (1981) [Theor. Math. Phys. **48**, 815 (1982)].
[50] M. Yu. Kuchiev, J. Phys. B **28**, 5093 (1995).